KIDNEY DISEASE

Activation of NRF2 ameliorates oxidative stress and cystogenesis in autosomal dominant polycystic kidney disease

Yi Lu[1]*, Yongzhan Sun[1]*, Zhiheng Liu[1]*, Yumei Lu[1], Xu Zhu[1], Bingxue Lan[1], Zeyun Mi[1], Lin Dang[1], Na Li[1], Wenlei Zhan[1], Lu Tan[2], Jingbo Pi[3], Hui Xiong[4†], Lirong Zhang[1†], Yupeng Chen[1†]

Oxidative stress is emerging as a crucial contributor to the pathogenesis of autosomal dominant polycystic kidney disease (ADPKD), but the molecular mechanisms underlying the disturbed redox homeostasis in cystic cells remain elusive. Here, we identified the impaired activity of the NRF2 (nuclear factor erythroid 2–related factor 2) antioxidant pathway as a driver of oxidative damage and ADPKD progression. Using a quantitative proteomic approach, together with biochemical analyses, we found that increased degradation of NRF2 protein suppressed the NRF2 antioxidant pathway in ADPKD mouse kidneys. In a cohort of patients with ADPKD, reactive oxygen species (ROS) frequently accumulated, and their production correlated negatively with NRF2 abundance and positively with disease severity. In an orthologous ADPKD mouse model, genetic deletion of *Nrf2* further increased ROS generation and promoted cyst growth, whereas pharmacological induction of NRF2 reduced ROS production and slowed cystogenesis and disease progression. Mechanistically, pharmacological induction of NRF2 remodeled enhancer landscapes and activated NRF2-bound enhancer-associated genes in ADPKD cells. The activation domain of NRF2 formed phase-separated condensates with MEDIATOR complex subunit MED16 in vitro, and optimal Mediator recruitment to genomic loci depended on NRF2 in vivo. Together, these findings indicate that NRF2 remodels enhancer landscapes and activates its target genes through a phase separation mechanism and that activation of NRF2 represents a promising strategy for restoring redox homeostasis and combatting ADPKD.

INTRODUCTION

Autosomal dominant polycystic kidney disease (ADPKD) is a common inherited kidney disease that affects 12.5 million people worldwide. Mutations in the *PKD1* or *PKD2* gene are the most common causes of ADPKD. ADPKD is characterized by the development of numerous bilateral renal cysts, which leads to progressive renal failure (*1*, *2*). Although the genetic basis of ADPKD is known, the molecular mechanisms responsible for the development of ADPKD remain poorly understood, and safer and more effective drugs are needed.

Accumulating evidence suggests that mitochondrial dysfunction is a key feature of ADPKD (*3*–*5*). Mitochondrial abnormalities, including altered mitochondrial membrane potential and abnormal mitochondrial morphology, are present in kidney tissues from both patients with ADPKD and animal models (*6*, *7*). Impairment of mitochondrial function results in the generation of reactive oxygen species (ROS), which are normally contained by the antioxidant defense system. An imbalance between ROS production and clearance leads to oxidative stress, which causes tissue damage and dysfunction (*8*, *9*). Evidence of decreased abundance of antioxidant enzymes and increased oxidative injury has been reported in nonorthologous PKD models (*10*). Recent clinical studies have shown that oxidative stress is present in patients with early-stage ADPKD and preserved renal function (*11*–*14*). These observations suggest that excessive ROS and increased oxidative stress are involved in ADPKD progression. However, the mechanisms underlying the dysregulation of antioxidant enzymes and the redox imbalance remain largely unknown, and it has not yet been shown that antioxidants can delay disease progression in ADPKD.

The transcription factor NRF2 (nuclear factor erythroid 2–related factor 2) was originally isolated as a homolog of the hematopoietic transcription factor NF-E2 p45 (*15*, *16*). NRF2 is recognized as a master regulator of cellular defenses against oxidative stress (*17*, *18*). NRF2 exerts its antioxidant function mainly through transcriptional activation of cytoprotective gene expression (*19*). The abundance of NRF2 is tightly controlled by two ubiquitin-proteasome degradation pathways. Under normal conditions, NRF2 is kept in the cytoplasm and binds to its canonical negative regulator kelch-like ECH-associated protein 1 (KEAP1) (*20*), which promotes NRF2 degradation through the Cullin 3 (CUL3) ubiquitin-proteasome system. A KEAP1-independent mechanism of NRF2 degradation is mediated by β-transducin repeats–containing protein (β-TrCP). Upon phosphorylation by glycogen synthase kinase–3β (GSK-3β), NRF2 binds to β-TrCP, which marks NRF2 for ubiquitination by the CUL1 E3 ubiquitin ligase complex. Disrupting the interaction between NRF2 and either KEAP1 or β-TrCP stabilizes NRF2 and promotes its translocation into the nucleus, where NRF2 binds to the antioxidant response element in the promoter regions of cytoprotective genes, recruits transcriptional coactivator proteins, and initiates target gene transcription (*17*).

Oxidative stress is now recognized as a major pathogenic factor for various progressive clinical and experimental renal diseases (*21*, *22*). Activation of NRF2 exerts protective effects by amelioration of oxidative injury and inflammation in various kidney diseases, including acute kidney injury, chronic kidney disease, and diabetic

[1]2011 Collaborative Innovation Center of Tianjin for Medical Epigenetics, Tianjin Key Laboratory of Medical Epigenetics, Key Laboratory of Immune Microenvironment and Disease (Ministry of Education), Department of Biochemistry and Molecular Biology, School of Basic Medical Sciences, Tianjin Medical University, Tianjin 300070, China. [2]Department of Laboratory Animal Science and Technology, Tianjin Medical University, Tianjin 300070, China. [3]School of Public Health, China Medical University, Shenyang 110122, China. [4]Department of Urology, Shandong Provincial Hospital affiliated to Shandong University, Jinan, Shandong, 250001, China.
*These authors contributed equally to this work.
†Corresponding author. Email: xionghui@sdu.edu.cn (H.X.); lzhang@tmu.edu.cn (L.Z.); ychen@tmu.edu.cn (Y.C.)

nephropathy, highlighting the NRF2 antioxidant pathway as an important target for kidney disease treatment (*23*, *24*).

In this study, we identified impaired activity of the NRF2 antioxidant pathway as a crucial contributor to oxidative stress and cystogenesis in ADPKD. We determined a regulatory mechanism by which NRF2 activates its target genes. We propose that pharmacological induction of NRF2 represents a promising strategy for the protection of kidney tissue from oxidative injury and for the treatment of ADPKD.

RESULTS

ROS accumulate in ADPKD kidneys and their production positively correlates with disease severity

Quantitative proteomics is an effective approach for comprehensively analyzing protein abundance under defined conditions. To understand the pathogenesis of and identify potential therapeutic targets for ADPKD, we used tandem mass tag–labeled, multiple-dimension liquid chromatography–tandem mass spectrometry to analyze kidney tissues from wild-type (WT) and $Pkd1^{-/-}$ mice with ADPKD (Fig. 1A). We detected and quantified 5100 proteins in these tissues, with 789 proteins up-regulated and 569 down-regulated in ADPKD kidneys (Fig. 1B). Gene Ontology (GO) analysis revealed that the up-regulated protein set was significantly enriched for proteins involved in inflammatory responses ($P < 0.001$), cellular metabolic processes ($P < 0.001$), collagen biosynthesis ($P < 0.001$), and the mitogen-activated protein kinase (MAPK) cascade ($P = 0.00128$) (fig. S1A), many of which play critical roles in ADPKD progression (*25*); the down-regulated protein set was significantly enriched for proteins involved in regulating oxidoreductase activity and the electron transport chain ($P < 0.001$; Fig. 1, C and D). Almost one-third of the proteins reduced abundance in ADPKD kidneys is located to mitochondria (Fig. 1E), indicating a prominent defect in mitochondrial functions. In addition, protein-protein interaction network analysis revealed that the down-regulated protein set was enriched for proteins involved in drug metabolic process, the citric acid cycle, respiratory electron transport, generation of precursor metabolites, and energy pathways (fig. S1B), all of which affect mitochondrial function (*26*, *27*). Collectively, our proteomic profiling revealed a prominent defect of mitochondrial function in ADPKD mouse kidneys.

One key feature of mitochondrial abnormality is excessive generation of ROS. Thus, we hypothesized that ROS accumulation occurs in ADPKD cells. To test this, we measured the ROS production in kidneys from ADPKD mice and human patients by dihydroethidium (DHE) staining. DHE staining was barely detectable in control tissues but was intense in kidney sections from both ADPKD mice (fig. S1C) and patients (Fig. 1F), indicating ROS accumulation in ADPKD kidneys. To determine the ROS status in kidney epithelial cells, we isolated *Dolichos biflorus* agglutinin (DBA)–positive collecting ducts, where cysts arise predominantly (*2*), from both WT and ADPKD mice and performed DHE staining. Cystic epithelial cells from the kidneys of ADPKD mice exhibited higher DHE staining than cells from the kidneys of WT mice (fig. S1D), confirming ROS accumulation in cyst-lining epithelial cells in ADPKD kidneys.

To evaluate whether the increase in ROS in ADPKD kidneys correlated with disease progression, we analyzed ROS status in kidneys from patients (table S1) with varying disease severity. We found that DHE intensity positively correlated with total kidney volume (Fig. 1G) and serum creatinine concentration (Fig. 1H), two key biomarkers of ADPKD severity (*2*). Thus, ROS accumulation correlated with disease progression.

NRF2 antioxidant signaling pathway is impaired in ADPKD kidneys

Through activation of genes encoding antioxidant and ROS-detoxifying enzymes, the NRF2 antioxidant pathway clears excess ROS and maintains redox homeostasis (*17*, *18*). To examine the activity of the NRF2 pathway, we inferred the expression of NRF2 targets from our proteomic data. We detected and quantified 38 proteins encoded by NRF2 target genes in our proteomic data (Fig. 2A). About 60% of these NRF2 targets were down-regulated in kidneys from ADPKD mice.

We did not detect NRF2 protein in our proteomic data; therefore, we analyzed the abundance of NRF2 by Western blotting. NRF2 abundance was decreased in kidney tissues and primary renal epithelial cells from ADPKD mice (Fig. 2, B and C). Analysis of NRF2 in the cytosolic and nuclear fractions showed a decrease in both compartments in ADPKD mouse kidneys (fig. S2). Consistent with the decrease of NRF2 protein abundance, the mRNA abundance of several well-characterized NRF2 target genes was markedly reduced in kidneys and primary cystic renal epithelial cells from ADPKD mice, including NAD(P)H (reduced form of nicotinamide adenine dinucleotide phosphate):quinone oxidoreductase 1 (encoded by *Nqo1*), glutamylcysteine synthetase (encoded by *Gcs*), superoxide dismutase 1 (encoded by *Sod1*), and superoxide dismutase 2 (encoded by *Sod2*) (Fig. 2, D and E). The similarity in *Nrf2* mRNA abundance between the WT and ADPKD mouse samples indicated that the reduction in NRF2 abundance mainly occurs at the post-transcriptional stage. Together, these results identified an impaired NRF2 antioxidant pathway in ADPKD kidneys.

To further validate the clinical relevance of the impaired NRF2 antioxidant pathway in ADPKD, we examined the NRF2 abundance in human patient samples (Fig. 2F). Decreased abundance of NRF2 correlated with increased ROS in patients with ADPKD (Fig. 2G). In addition, we also observed that NRF2 abundance inversely correlated with total kidney volume and serum creatinine concentration (Fig. 2, H and I) and positively correlated with estimated glomerular filtration rate (eGFR) (Fig. 2J), indicating a correlation between the impaired NRF2 antioxidant pathway and ADPKD severity.

Loss of *Nrf2* increases oxidative stress and accelerates cyst growth in an orthologous ADPKD mouse model

To explore the role of NRF2 in ADPKD progression in vivo, we crossed *Nrf2* knockout mice with *Pkd1* knockout mice. To initiate cystogenesis, we induced *Pkd1* deletion by tamoxifen injection at postnatal day 10 (P10) and euthanized the animals 12 days later to collect the kidneys (Fig. 3A). In mice with functional *Pkd1*, neither heterozygous nor homozygous loss of *Nrf2* ($Pkd1^{+/+};Nrf2^{+/-}$ or $Pkd1^{+/+};Nrf2^{-/-}$) resulted in apparent abnormalities in kidney size, kidney weight–to–body weight ratio, or blood urea nitrogen (BUN) (Fig. 3, B to D), suggesting that the loss or reduced function of *Nrf2* alone has little effect on kidney development and renal function. However, deletion of *Nrf2* in $Pkd1^{-/-}$ mice ($Pkd1^{-/-};Nrf2^{-/-}$) resulted in markedly larger kidney size; higher kidney weight–to–body weight ratio, BUN, and serum creatinine concentration; increased cyst formation; and higher cystic index (Fig. 3, B to F, and fig. S3A). We evaluated ROS abundance using DHE and ROS-induced damage

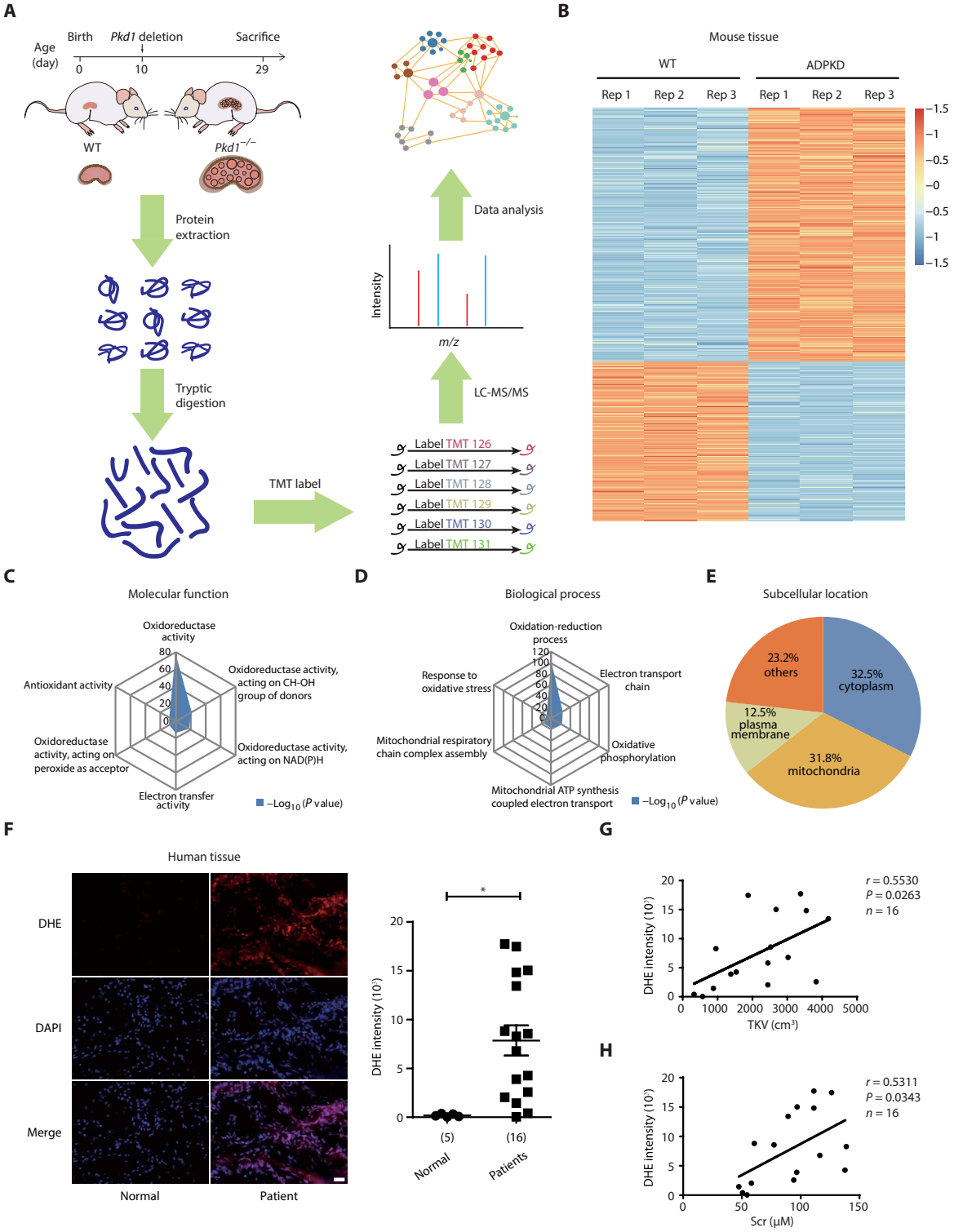

Fig. 1. Accumulation of ROS positively correlates with disease progression in ADPKD. (**A**) Schematic overview of the proteomic analysis. *m/z*, mass/charge ratio; LC-MS/MS, liquid chromatography–tandem mass spectrometry. (**B**) Heatmap of protein abundance values from kidneys from WT and early-onset ADPKD mice. Proteomic analysis was performed with kidneys from three mice of each genotype. Data for each biological replicate are shown. (**C** and **D**) Gene Ontology (GO) enrichment analyses of the down-regulated proteins. ATP, adenosine 5′-triphosphate. (**E**) Subcellular location of the down-regulated proteins in ADPKD kidneys. (**F**) Immunofluorescence analysis (left) and quantification (right) of ROS production as measured by DHE intensity in human kidneys. Scale bar, 50 μm. (**G**) Correlation between DHE intensity and total kidney volume (TKV) for patients with ADPKD. (**H**) Correlation between DHE intensity and serum creatinine (Scr) for patients with ADPKD. Data represent means ± SEM. *$P < 0.05$. Two-tailed unpaired Student's *t* test was used for statistical analysis in (F). Pearson's correlation coefficients are displayed in (G) and (H); *P* values were determined using linear regression analysis.

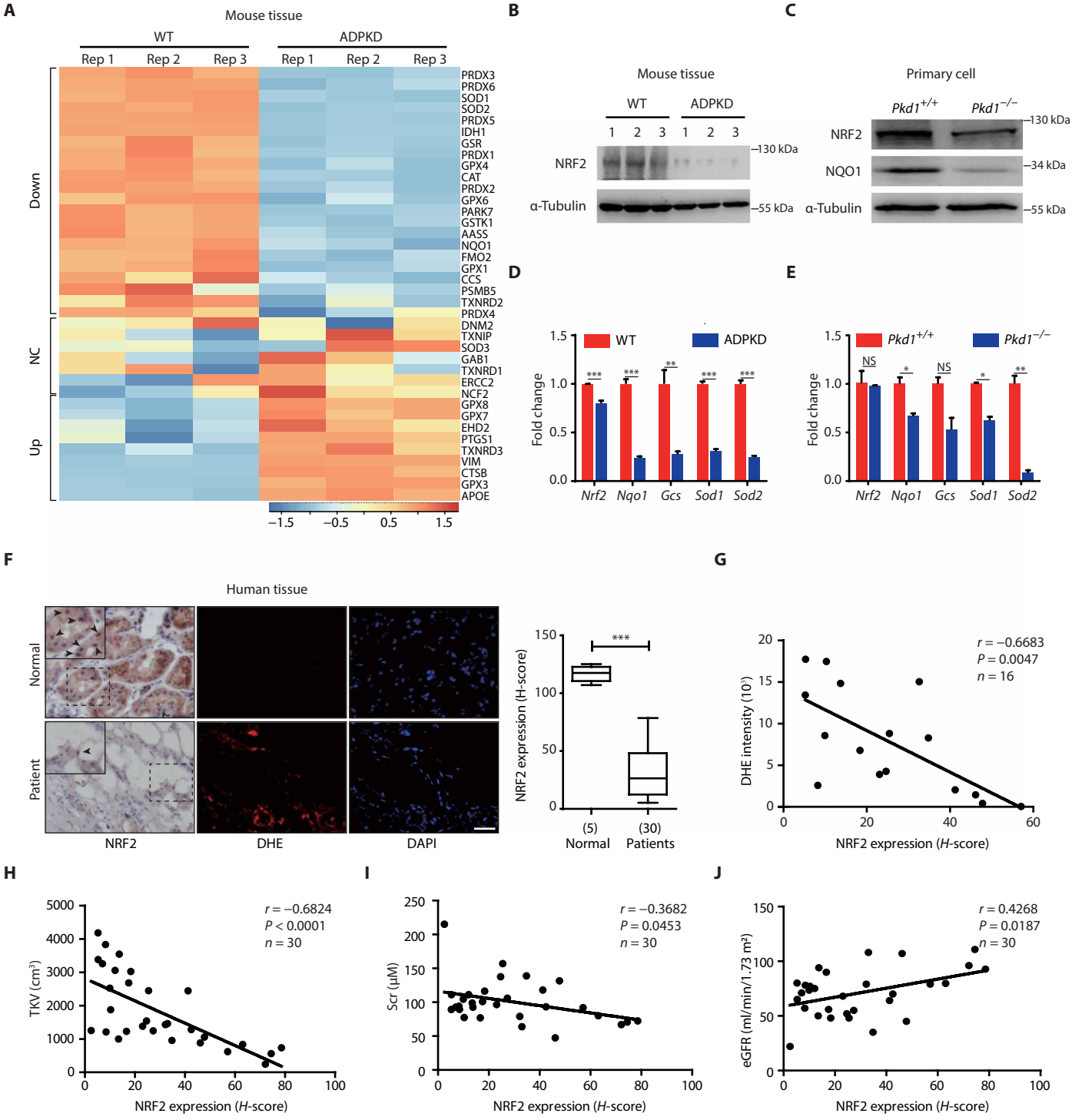

Fig. 2. Impaired activity of NRF2 antioxidant pathway in ADPKD kidneys. (**A**) Quantitative proteomic analysis of NRF2 targets in kidneys from WT and early-onset *Pkd1*$^{-/-}$ mice. Results from three mice for each are shown. NC, not changed. (**B**) Western blot analysis of NRF2 abundance in WT and *Pkd1*$^{-/-}$ kidneys. The numbers under WT and ADPKD indicate tissue from separate mice. (**C**) Western blot analysis of NRF2 and NQO1 in DBA-isolated primary cells from *Pkd1*$^{+/+}$ and *Pkd1*$^{-/-}$ mouse kidneys. (**D**) RT-qPCR analysis of the change in mRNA abundance of *Nrf2* and its indicated targets in WT and *Pkd1*$^{-/-}$ kidney tissues. (**E**) RT-qPCR analysis of the change in mRNA abundance of *Nrf2* and its targets in DBA-positive primary cells from *Pkd1*$^{+/+}$ and *Pkd1*$^{-/-}$ mouse kidneys. (**F**) Immunohistochemistry staining of NRF2 and immunofluorescence of ROS in kidney tissue from normal and patients with ADPKD. Scale bar, 50 μm. Arrowheads indicate positive nuclear staining of NRF2. Insets show a higher magnification of the dashed rectangular areas. NRF2 abundance was quantified using *H*-score from the immunohistochemistry data. DAPI, 4′,6-diamidino-2-phenylindole. (**G** to **J**) Correlation between NRF2 abundance (*H*-score) in kidney tissues with various parameters of kidney function: DHE intensity (G), total kidney volume (TKV) (H), serum creatinine (I), and eGFR (J). Data represent means ± SEM. **P* < 0.05, ***P* < 0.01, and ****P* < 0.001; NS, not significant. Two-tailed unpaired Student's *t* test was used for statistical analysis in (D to F). Pearson's correlation coefficients are displayed in (G to J); *P* values were determined using linear regression analysis.

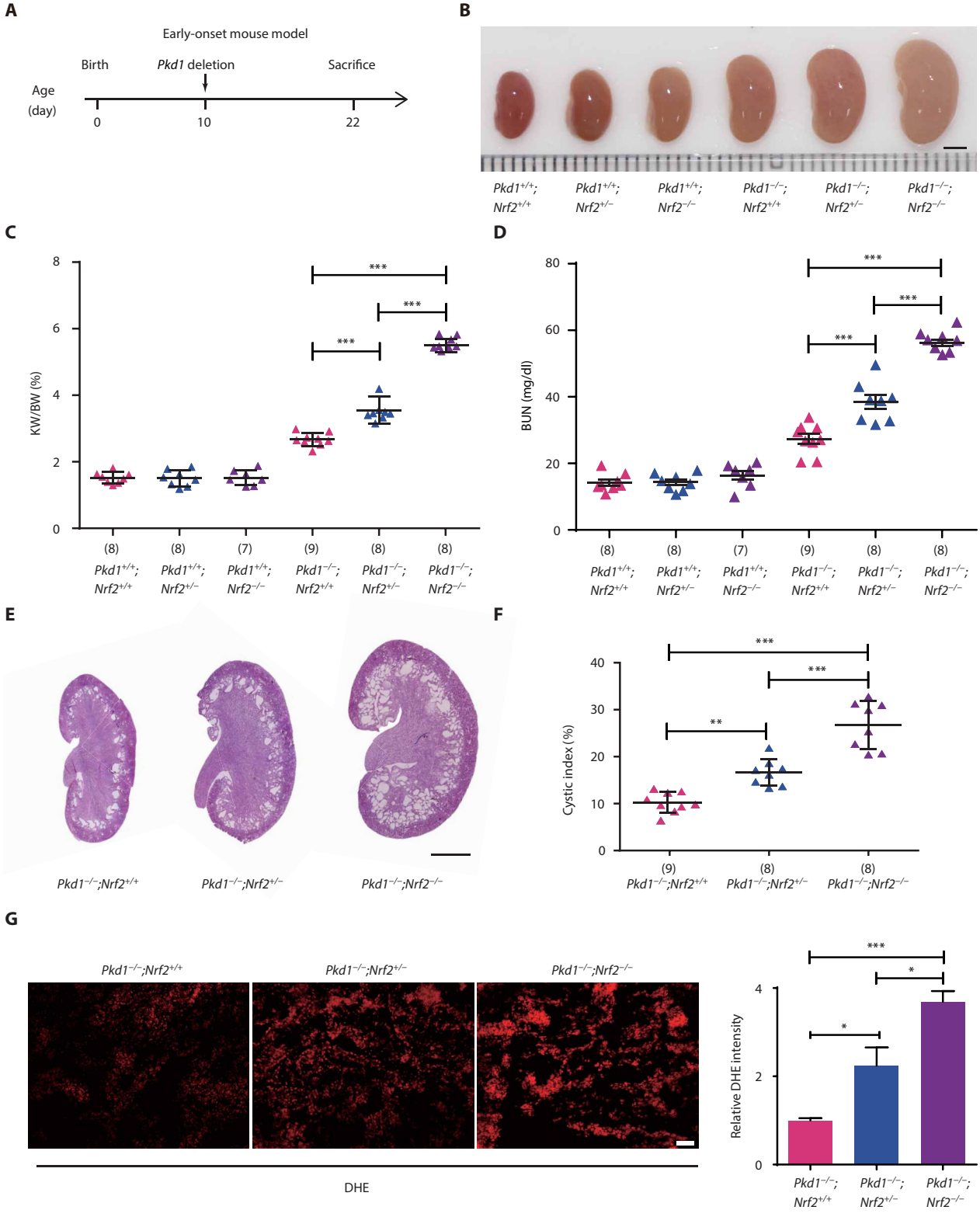

Fig. 3. Genetic depletion of *Nrf2* increases oxidative injury and accelerates cystogenesis in ADPKD mouse model. (**A**) Schematic diagram of the experimental design in the *Pkd1*$^{-/-}$;*Nrf2*$^{-/-}$ mouse model. (**B**) Representative images of P22 kidneys from the indicated groups of mice. (**C**) Kidney weight–to–body weight (KW/BW) ratios in the indicated groups. (**D**) BUN concentration in the indicated groups. (**E**) Hematoxylin and eosin (H&E) staining of mouse kidney sections from the indicated groups. (**F**) Cystic index quantified from H&E images. (**G**) DHE staining (left) and quantification (right) of frozen mouse kidney sections. Scale bars, 2 mm (B and E) and 50 μm (G). Data represent means ± SEM. *$P < 0.05$, **$P < 0.01$, and ***$P < 0.001$. Data for each mouse is indicated with the number of mice indicated in parentheses (C, D, and F) or data are from kidneys from three mice (G). Two-tailed unpaired Student's *t* test was used for statistical analysis.

by staining for 8-hydroxy-2′-deoxyguanosine (8-OHdG). Both were increased in ADPKD mice with *Nrf2* deletion (Fig. 3G and fig. S3B). We also observed increased cell proliferation [based on proliferating cell nuclear antigen (PCNA) staining] and expression of inflammatory genes (*Mcp1* and *Il-6*) in $Pkd1^{-/-};Nrf2^{-/-}$ mice (fig. S3, C and D). Collectively, these results showed that loss of NRF2 exacerbates ADPKD severity.

Activation of NRF2 ameliorates oxidative damage and cystogenesis in the early- and late-onset ADPKD mouse models

Because we observed that NRF2 is down-regulated in ADPKD mouse and human kidneys and genetic disruption of *Nrf2* in mice worsens ADPKD, we hypothesized that induction of NRF2 can slow disease progression. Sulforaphane (SFN), a natural compound derived from cruciferous vegetables, is an inhibitor of KEAP1 that disrupts KEAP1-NRF2 complex and, thus, promotes nuclear accumulation of NRF2 (*28*). SFN has been used in basic research and clinical studies for cancer and other chronic diseases (*29*). We therefore examined the effects of SFN-mediated NRF2 activation on cystogenesis and renal function in ADPKD animal models.

To generate the early-onset mouse model, we induced *Pkd1* gene deletion by a single injection of tamoxifen at P10 and initiated SFN treatment at P11, which was continued for 3 weeks (Fig. 4A). SFN treatment decreased the kidney size, cystic index, kidney weight–to–body weight ratio, and ROS accumulation and improved renal function in $Pkd1^{-/-};Nrf2^{+/+}$ mice and $Pkd1^{-/-};Nrf2^{+/-}$ mice but not in $Pkd1^{-/-};Nrf2^{-/-}$ mice (Fig. 4, B to F, and fig. S4, A and B). We also observed decreased cell proliferation upon SFN treatment (fig. S4C). The expression of three NRF2 target genes, *Sod1*, *Gcs*, and *Prdx*, was increased in response to SFN treatment in an NRF2-dependent manner (fig. S4D), suggesting that SFN treatment increases NRF2 activity in the ADPKD mouse kidney. Together, these results showed that SFN reduces oxidative stress in kidney tissue and attenuates ADPKD pathogenesis through a mechanism dependent on the NRF2 pathway.

To more closely mimic disease progression in patients with ADPKD and to evaluate the long-term effects of SFN treatment, we used a late-onset ADPKD mouse model and addressed whether SFN reduced cyst growth in mice with established ADPKD (*30*). We induced *Pkd1* gene deletion by two tamoxifen injections at P25 and P28. SFN treatment was initiated 1 month later (P55; $T = 0$ month) and continued for 2 months before the mice were euthanized (Fig. 4G). To follow disease progression longitudinally, we imaged the kidneys of each group of ADPKD mice by magnetic resonance imaging (MRI) at $T = 0$ months (P55), $T = 1$ month (P85), and $T = 2$ months (P115) (Fig. 4H). We found that SFN treatment substantially inhibited cyst growth in ADPKD mice, as indicated by the MRI image-based total kidney volume calculation (Fig. 4, H and I). Moreover, SFN treatment also resulted in a marked decrease of the cystic index and kidney size (Fig. 4, J and K, and fig. S4F), kidney weight–to–body weight ratio (fig. S5G), ROS accumulation (fig. S4H), improved renal function (Fig. 4L), and decreased cell proliferation (fig. S4I). The expression of three NRF2 target genes, *Sod1*, *Gcs*, and *Prdx*, was increased in response to SFN treatment (fig. S4J), suggesting that SFN treatment increases NRF2 activity in the late-onset ADPKD model. We observed no apparent systemic toxicity, such as behavioral change and body weight loss (fig. S4K), in SFN-treated control mice, indicating a high degree of biosafety for SFN treatment.

ADPKD is a systemic disorder with multiple clinical manifestations. Besides the kidneys, cysts also occur in other organs, such as the liver, arachnoid membrane, pancreas, and seminal vesicles. Polycystic liver disease is considered as the most frequent extrarenal manifestation of ADPKD and is characterized by a continuous increase in the number and volume of cysts (*31*). Therefore, we also examined the effects of SFN treatment on liver cyst growth in the late-onset ADPKD mouse model. SFN treatment was initiated 1 month after the deletion of *Pkd1* gene (P55; $T = 0$ months) and continued for 2 months before the mice were euthanized. The number and volume of liver cysts were markedly decreased by SFN treatment (fig. S4, L to N). Together, these findings suggest that SFN is a potentially safe candidate for ADPKD treatment with effectiveness in inhibiting cystogenesis in both kidney and liver.

GSK-3β inhibition delays cyst growth in an NRF2-dependent manner

Our data indicated that NRF2 abundance was decreased in ADPKD kidneys due to a posttranscriptional mechanism (Fig. 2, B to E). NRF2 abundance is tightly regulated by the KEAP1-CUL3 and β-TrCP–CUL1 ubiquitin-proteasome degradation systems. The latter is influenced by GSK-3β, which phosphorylates NRF2 and enables NRF2 to bind to β-TrCP. To explore the roles of these two degradation pathways in the regulation of NRF2 abundance, we first analyzed the abundance of KEAP1 and GSK-3β in kidneys from WT and the early-onset ADPKD mice. We found that both KEAP1 and GSK-3β were increased in ADPKD kidneys (Fig. 5A), suggesting that the repression of NRF2 is caused by the dysregulation of its degradation pathways.

Our GSK-3β results are consistent with a previous study of ADPKD kidneys, which also found an increase in this kinase and reported that inhibition of kinase activity by the selective inhibitor, 4-benzyl-2-methyl-1,2,4-thiadiazolidine-3,5-dione (TDZD-8), slows cyst development in an orthologous ADPKD mouse model (*32*). Because GSK-3β directly phosphorylates NRF2 and induces its degradation, we hypothesized that activation of the NRF2 pathway contributes to the beneficial effects of GSK-3β inhibition on cystogenesis. We tested this hypothesis in the early-onset mouse model (Fig. 5B). TDZD-8 treatment substantially reduced kidney size (Fig. 5C), cystic index (Fig. 5, D and E), kidney weight–to–body weight ratio (Fig. 5F), and ROS accumulation (Fig. 5H) and improved kidney function (Fig. 5G and fig. S5A) in $Pkd1^{-/-};Nrf2^{+/+}$ but not in $Pkd1^{-/-};Nrf2^{-/-}$ mice. Consistent with the functional data, the abundance of NRF2 and the expression of its targets were increased in TDZD-8–treated $Pkd1^{-/-};Nrf2^{+/+}$ mice but not in $Pkd1^{-/-};Nrf2^{-/-}$ mice (Fig. 5I and fig. S5B). Together, these results showed that NRF2 is required for the suppression of cystogenesis by GSK-3β inhibition.

Pharmacological induction of NRF2 promotes enhancer activation in ADPKD cells

NRF2 is the master transcription factor in cellular defense against oxidative stress, and this function is mainly mediated through transcriptional activation of its cytoprotective target genes. To explore the transcriptional regulatory mechanisms underlying the protective roles of NRF2 in ADPKD, we performed chromatin immunoprecipitation followed by chromatin immunoprecipitation–sequencing (ChIP-seq) to analyze the genome-wide distribution of NRF2 in WT 9-12 human ADPKD cells. We found that SFN

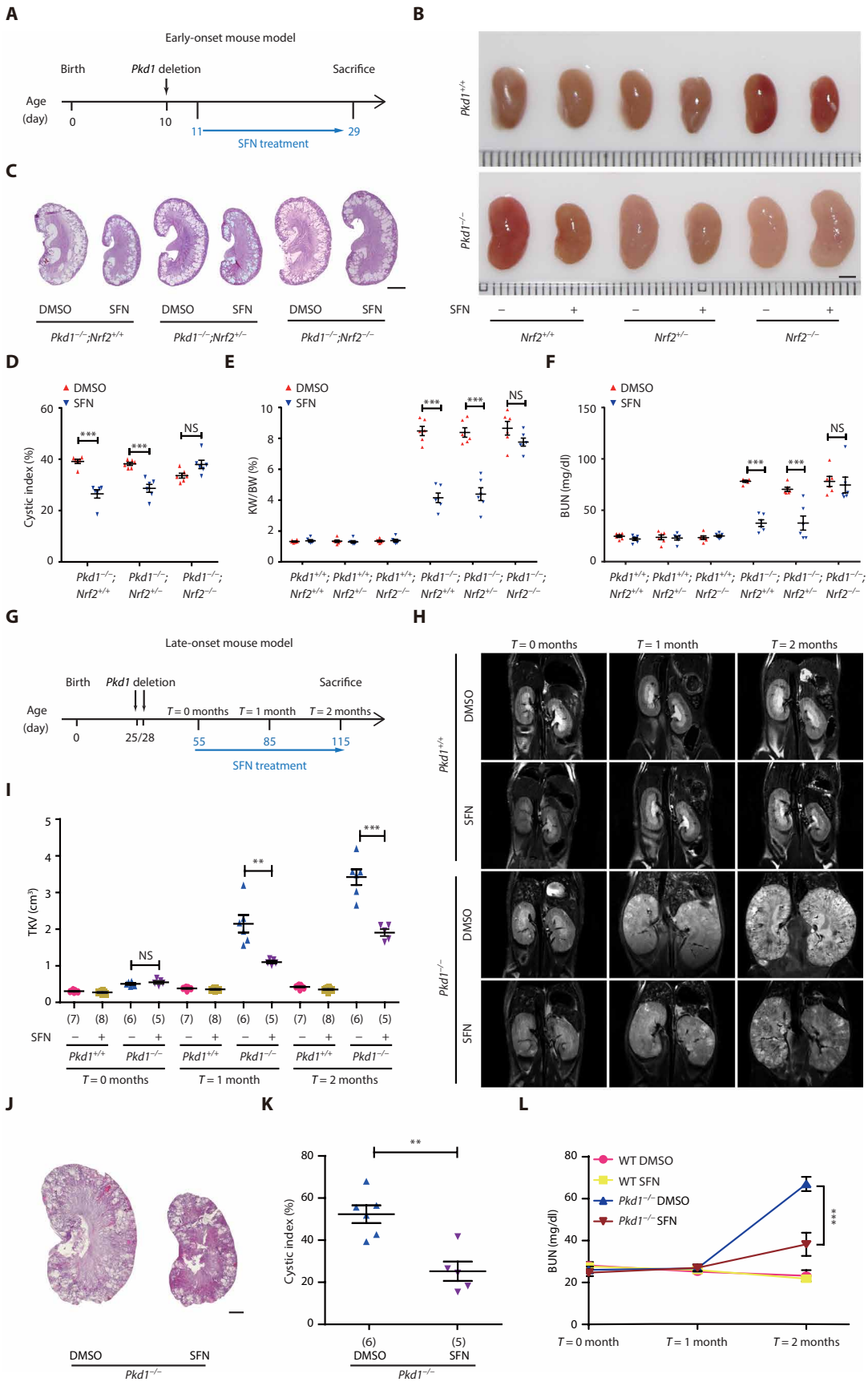

Fig. 4. Activation of NRF2 inhibits cyst development in the early- and late-onset ADPKD mouse models. (**A**) Outline of the experimental design in the early-onset ADPKD mouse model. Mice not receiving SFN were administered vehicle (DMSO, dimethyl sulfoxide). (**B**) Representative images of P29 kidneys from the indicated groups of mice. (**C**) H&E-stained kidney sections from P29 mice treated with DMSO or SFN. (**D**) Graph of the cystic index at P29 of the indicated groups. (**E**) Ratios of kidney weight–to–body weight at P29 in the indicated groups. (**F**) Graph of the concentration of BUN at P29 in the indicated groups. (**G**) Schematic diagram of experimental design in the late-onset ADPKD mouse model. Mice not receiving SFN were administered vehicle (DMSO). (**H**) Representative magnetic resonance imaging (MRI) images of kidneys from the indicated genotype and treatment groups. (**I**) Total kidney volume calculated from MRI slides acquired at the indicated time points from mice in the indicated groups. (**J**) Representative H&E sections from *Pkd1*$^{-/-}$ mice treated with DMSO or SFN. (**K**) Cystic index of kidneys from mice treated with DMSO or SFN. (**L**) Graph showing BUN concentration at the indicated time points. Number of mice is the same as in (I). Scale bars, (B, C, and J) 2 mm. Data for each mouse are plotted. Each group contained six mice in (D to F) or the number of mice in each group is indicated in parentheses (I and K). Data represent means ± SEM. $^{**}P < 0.01$ and $^{***}P < 0.001$. Two-tailed unpaired Student's *t* test was used for statistical analysis.

treatment substantially increased NRF2 occupancy on chromatin, with peak numbers rising from 418 to 2168 binding sites, but that SFN treatment had little effect on the relative proportions of genomic regions occupied by NRF2 (Fig. 6A). Our results are consistent with previous studies (*33*, *34*) showing that only 4% of NRF2 binding is located in promoter regions and that most (>95%) occurs in intergenic

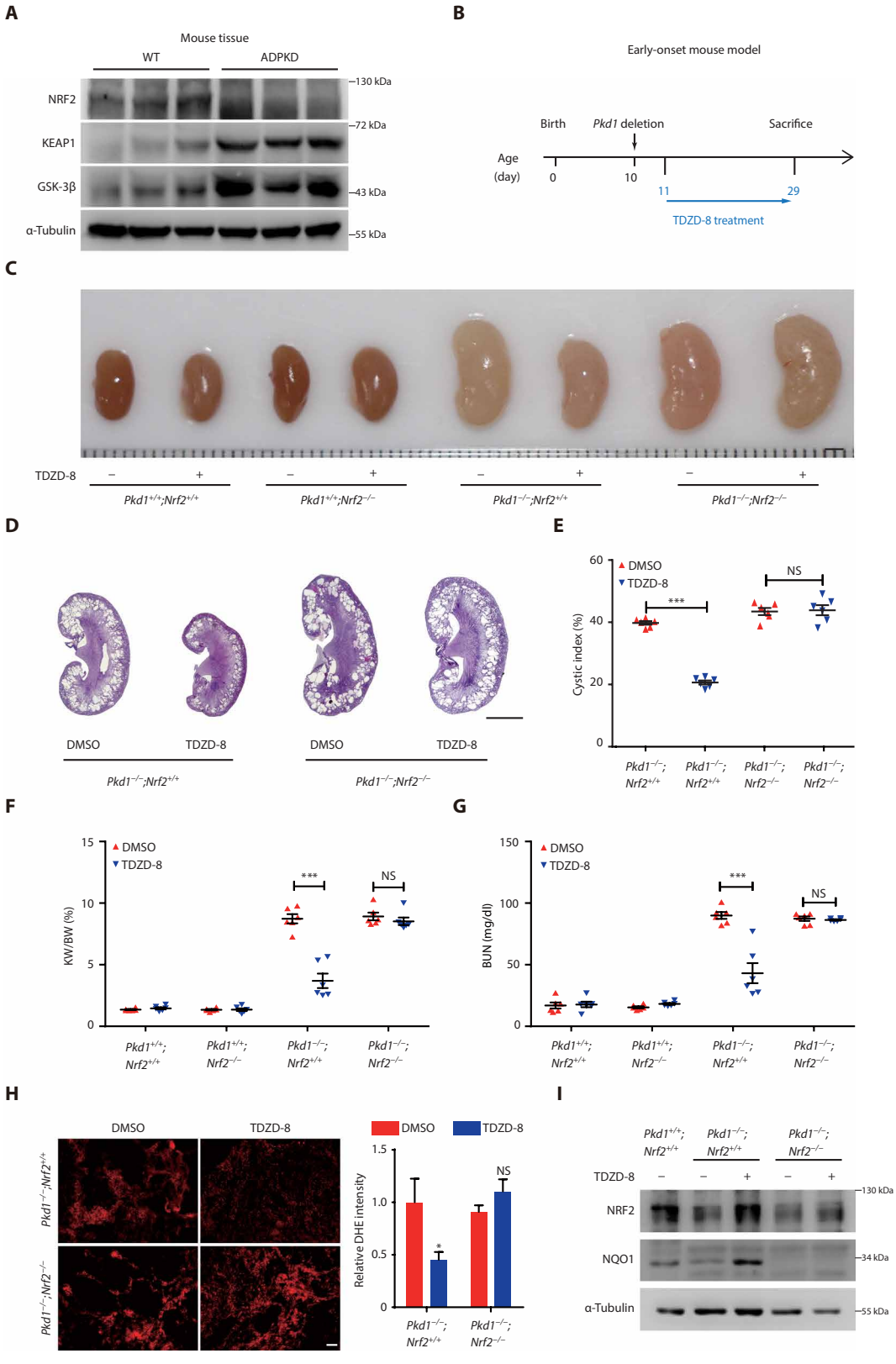

Fig. 5. GSK-3β inhibition ameliorates ADPKD progression through induction of NRF2. (**A**) Western blot of NRF2, KEAP1, and GSK-3β in kidneys from WT and *Pkd1*$^{-/-}$ mice. Each lane represents a sample from an independent mouse. (**B**) Outline of the experimental design. Mice not receiving SFN were administered vehicle (DMSO). (**C**) Representative images of P29 kidneys from mice in the indicated groups. (**D**) H&E staining of kidneys from the indicated groups. (**E**) Graph of the cystic index calculated from the H&E sections such as those in (D). (**F** and **G**) Kidney weight–to–body weight ratios and BUN concentration in the indicated groups. (**H**) DHE staining and quantification of kidney sections from three mice in each of the indicated groups. (**I**) Western blot analysis of NRF2 and NQO1 in the indicated groups. Scale bars, 2 mm (C and D) and 50 μm (H). Data for each mouse are plotted and each group contained six mice in (E to G). Data represent means ± SEM. *$P < 0.05$ and ***$P < 0.001$. Two-tailed unpaired Student's *t* test was used for statistical analysis.

or intragenic regions. The mechanisms and functions of NRF2 binding at these extrapromoter genomic sites are largely unknown (*19*).

To explore the relationship between NRF2 binding and its transcriptional activity, we characterized the chromatin features of NRF2 binding sites. We examined key active histone markers that define genome-wide regulatory regions, including acetylated H3K27 (H3K27ac), monomethylated H3K4 (H3K4me1), and trimethylated H3K4 (H3K4me3) (*35*). Promoters of actively transcribed genes are marked by H3K4me3 and H3K27ac, whereas active enhancers are enriched for H3K4me1 and H3K27ac. We performed ChIP-seq analyses of these histone modifications and examined the interaction between NRF2 binding and its surrounding chromatin context. SFN treatment of WT 9-12 increased H3K27ac signals at NRF2-bound regions while slightly reducing the genome-wide average H3K27ac signal (Fig. 6, B and C). We did not detect genome-wide changes in H3K4me1 (Fig. 6, B and D) or H3K4me3 (Fig. 6, B and E) occupancy in response to SFN nor did we detect noticeable changes in these

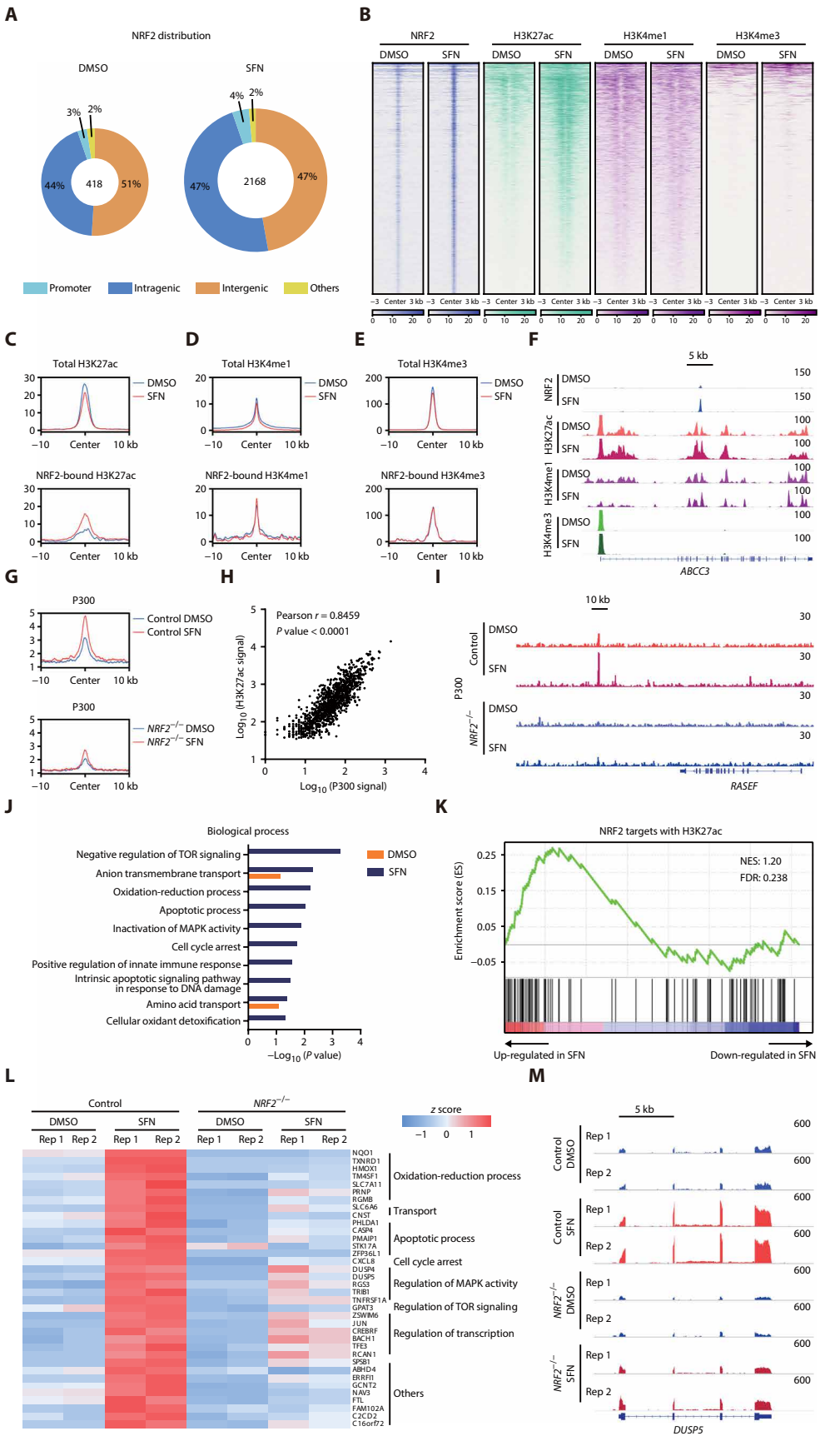

Fig. 6. NRF2 regulates transcription through enhancer activation. (**A**) Genomic distribution of NRF2 in WT 9-12 cells treated with DMSO or SFN. The numbers represent sites occupied by NRF2. (**B**) Heatmaps of normalized ChIP-seq signals for NRF2, H3K27ac, H3K4me1, and H3K4me3. The rows show 3 kb around the NRF2 peak center. (**C** to **E**) Composite plots of normalized ChIP-seq signals for H3K27ac (C), H3K4me1 (D), and H3K4me3 (E) in the whole genome (total) or in regions occupied by NRF2 in WT 9-12 cells treated with DMSO or SFN. (**F**) ChIP-seq tracks of NRF2, H3K27ac, H3K4me1, and H3K4me3 in the genomic region near *ABCC3*. (**G**) Composite plots of normalized ChIP-seq signals for P300. (**H**) Correlation analysis between P300 and H3K27ac signals. (**I**) ChIP-seq tracks of P300 at genomic regions near *RASEF*. (**J**) GO analysis of NRF2 target genes induced by SFN. TOR, target of rapamycin. (**K**) GSEA of H3K27ac at NRF2 target genes. FDR, false discovery rate; NES, normalized enrichment score. (**L**) Heatmap of NRF2 target expression values. Data from two independent experiments are shown. (**M**) RNA-seq tracks of *DUSP5* in the cells in the indicated groups.

chromatin marks at NRF2-bound regions upon SFN treatment. Inspection of the track profiles for different histone modifications indicated that the change in H3K27ac was primarily occurring in enhancer regions and that NRF2 was bound at an enhancer site, as seen by the representative tracks of the *ABCC3* gene in Fig. 6F.

To determine whether the redistribution of H3K27ac observed in response to SFN required NRF2, we knocked out *NRF2* in WT 9-12 cells ($NRF2^{-/-}$ cells) by CRISPR-Cas9–mediated gene editing (table S2). The abundance of SFN-induced NRF2 was markedly decreased in $NRF2^{-/-}$ cells (fig. S6A). We performed ChIP-seq analysis of H3K27ac in $NRF2^{-/-}$ cells treated with vehicle or SFN. In contrast to WT cells, SFN treatment had negligible effects on H3K27ac at NRF2-bound regions (fig. S6B). Analysis of various antioxidant genes showed that NRF2 is required for the increase of H3K27ac signal at both enhancers (fig. S6C) and promoters (fig. S6D).

NRF2 binds to histone acetyltransferase P300, which deposits H3K27ac (*36*). Thus, we hypothesized that NRF2-dependent enhancer remodeling is linked to the recruitment

of P300. We found that NRF2 colocalized with P300 after SFN treatment and that the occupancy of P300 was markedly decreased in cells lacking NRF2 (Fig. 6G). The intensity of P300 signal significantly correlated with that of H3K27ac signal (Fig. 6H). The dependence of SFN-stimulated redistribution of P300 binding to chromatin on NRF2 was evident by inspection of the tracks, as seen in the representative data for *RASEF* in Fig. 6I. These results suggested that NRF2 recruits P300 to facilitate the acetylation of H3K27 at NRF2-bound enhancers.

GO analysis of genes associated with NRF2-bound active enhancers in SFN-treated cells revealed that the genes were highly enriched for ADPKD-associated pathways, such as pathways regulating TOR (target of rapamycin) signaling, cell cycle, MAPK activity, apoptotic processes, and oxidative stress (Fig. 6J). Collectively, these data suggested that activation of NRF2 remodels the enhancer landscape and promotes enhancer activation in ADPKD cells.

We investigated whether the NRF2-induced increase of chromatin marks associated with enhancer activity leads to the activation of the associated genes in ADPKD cells. Gene set enrichment analysis (GSEA) revealed that genes associated with NRF2-bound enhancers were enriched for genes up-regulated by SFN (Fig. 6K). Intersection of the genes up-regulated by SFN with genes associated with NRF2-bound active enhancers yielded 36 genes (Fig. 6L). Analysis of the effect of SFN on the expression of these 36 genes showed that these genes were strongly activated by SFN treatment in parental WT 9-12 cells and that this activation was diminished in *NRF2* knockout cells, indicating that they are indeed NRF2 target genes. Representative RNA sequencing (RNA-seq) track profiles for *DUSP5* clearly shows this dependence on NRF2 for SFN-induced expression (Fig. 6M).

We also examined the expression of five redox-related genes from the set of 36 genes in ADPKD mouse kidneys. Expression of these genes was decreased in kidneys from *Pkd1*$^{-/-}$ mice with late-onset ADPKD, and SFN treatment partially restored expression (fig. S6E). Furthermore, expression of these genes was increased in SFN-treated *Pkd1*$^{-/-}$;*Nrf2*$^{+/+}$ mice but not in *Pkd1*$^{-/-}$;*Nrf2*$^{-/-}$ mice with early-onset ADPKD, suggesting that NRF2 is required for SFN-induced expression (fig. S6F). Together, these data indicated that SFN stimulated NRF2 to activate enhancer-associated cytoprotective genes in cystic cells.

Phase separation of NRF2 with MED16 occurs in vitro

Accumulating evidence suggests that phase separation is a key regulatory mechanism for transcriptional control (*37*). The activation domains (ADs) of several transcription factors form phase-separated condensates with the Mediator complex at enhancers (*38*). Because our data revealed preferential binding of NRF2 to enhancers, we hypothesized that NRF2 forms phase-separated condensates at enhancers, thereby promoting the activation of its enhancer-associated target genes.

A key feature of proteins involved in phase separation is the presence of intrinsically disordered regions (IDRs) (*39*). Sequence analysis revealed that NRF2 has three predicted IDRs (Fig. 7A). To investigate whether these IDRs form phase-separated droplets in vitro, we purified a peptide containing the first IDR (NRF2$^{1\text{-}208}$) and a peptide containing the second and third IDRs (NRF2$^{209\text{-}605}$), each tagged with mEGFP (monomeric enhanced green fluorescent protein) (Fig. 7B). Droplet formation assays revealed that both NRF2$^{1\text{-}208}$-mEGFP and NRF2$^{209\text{-}605}$-mEGFP formed phase-separated droplets in a concentration-dependent manner (Fig. 7C). NRF2$^{1\text{-}208}$-mEGFP also contains the AD of NRF2 and formed markedly larger droplets than NRF2$^{209\text{-}605}$-mEGFP at the same concentration. We tested the fluid properties of the condensates using fluorescence recovery after photobleaching (FRAP). Consistent with the droplet formation assays, FRAP experiments showed that NRF2$^{1\text{-}208}$-mEGFP signal recovered within 30 s (Fig. 7D), whereas the recovery of NRF2$^{209\text{-}605}$-mEGFP signals took more than 10 min (fig. S7A). Consistent with the FRAP analysis, fusion analysis showed that NRF2$^{1\text{-}208}$ droplets fused into one droplet within seconds (Fig. 7E). These results indicated that NRF2$^{1\text{-}208}$-mEGFP droplets are dynamic and liquid-like, whereas NRF2$^{209\text{-}605}$-mEGFP droplets had relatively poor dynamics and droplet formation.

The AD of NRF2 activates gene transcription by recruiting the Mediator complex through an interaction with the MED16 subunit (*40*). Sequence analysis revealed that MED16 does not contain predicted IDRs. To test whether MED16 can incorporate into NRF2 phase-separated condensates, we purified a recombinant N-terminal portion of mCherry-fused MED16 (mCherry-MED16-N) (fig. S7B). This MED16 peptide contains residues 1 to 212, which are responsible for the interaction with NRF2 (*40*). NRF2$^{1\text{-}208}$ formed micrometer-sized droplets at 10 μM (Fig. 7C), whereas MED16 failed to form droplets at this concentration in the presence of mEGFP (Fig. 7F). However, when we mixed these two recombinant proteins together, they formed double-positive, spherical droplets (Fig. 7F), suggesting that NRF2$^{1\text{-}208}$ condensates incorporate and concentrate MED16 in vitro.

To determine the role of IDRs in NRF2 gene transactivation, we examined the effects of IDR mutants on NRF2 target gene expression. We expressed either full-length NRF2 fused to EGFP or the NRF2 peptide lacking the first IDR (EGFP-NRF2$^{209\text{-}605}$) in *NRF2* knockout cells (fig. S7C). Only full-length NRF2 increases the expression of NRF2 target genes (Fig. 7G), suggesting that the first IDR is required for NRF2 transactivation.

NRF2 forms nuclear condensates with Mediator complex at superenhancers

The Mediator complex forms nuclear condensates and concentrates transcriptional machinery in cells (*41*). Because we found that NRF2 associates with and forms phase-separated condensates with a component of the Mediator complex in vitro, we evaluated whether NRF2 forms nuclear condensates with Mediator in vivo. MED1, the largest subunit of the Mediator complex, is a good surrogate for Mediator condensates in vivo (*41*). We detected NRF2-positive nuclear puncta in WT 9-12 ADPKD cells, and the size and the number of NRF2-positive puncta increased upon SFN treatment (Fig. 8A). Costaining for NRF2 and MED1 showed that they partially colocalized at puncta in the nuclei of cells (Fig. 8B), suggesting that NRF2 associates with Mediator condensates in vivo.

The Mediator complex mainly forms phase-separated condensates at superenhancers (*41*). Superenhancers are clusters of enhancers that assemble a high density of transcriptional coactivator proteins and drive robust expression of genes, some of which are critical for cell identity or disease progression (*42*, *43*). We characterized the superenhancer landscape in WT 9-12 cells with or without SFN treatment. We ranked the enhancers according to their H3K27ac signals, classifying those with H3K27ac signal intensity above the inflection point as superenhancers. SFN treatment doubled the number of superenhancers, from 294 in control cells to 581 superenhancers in SFN-treated cells (Fig. 8C). The proportion of NRF2-bound superenhancers increased substantially upon SFN

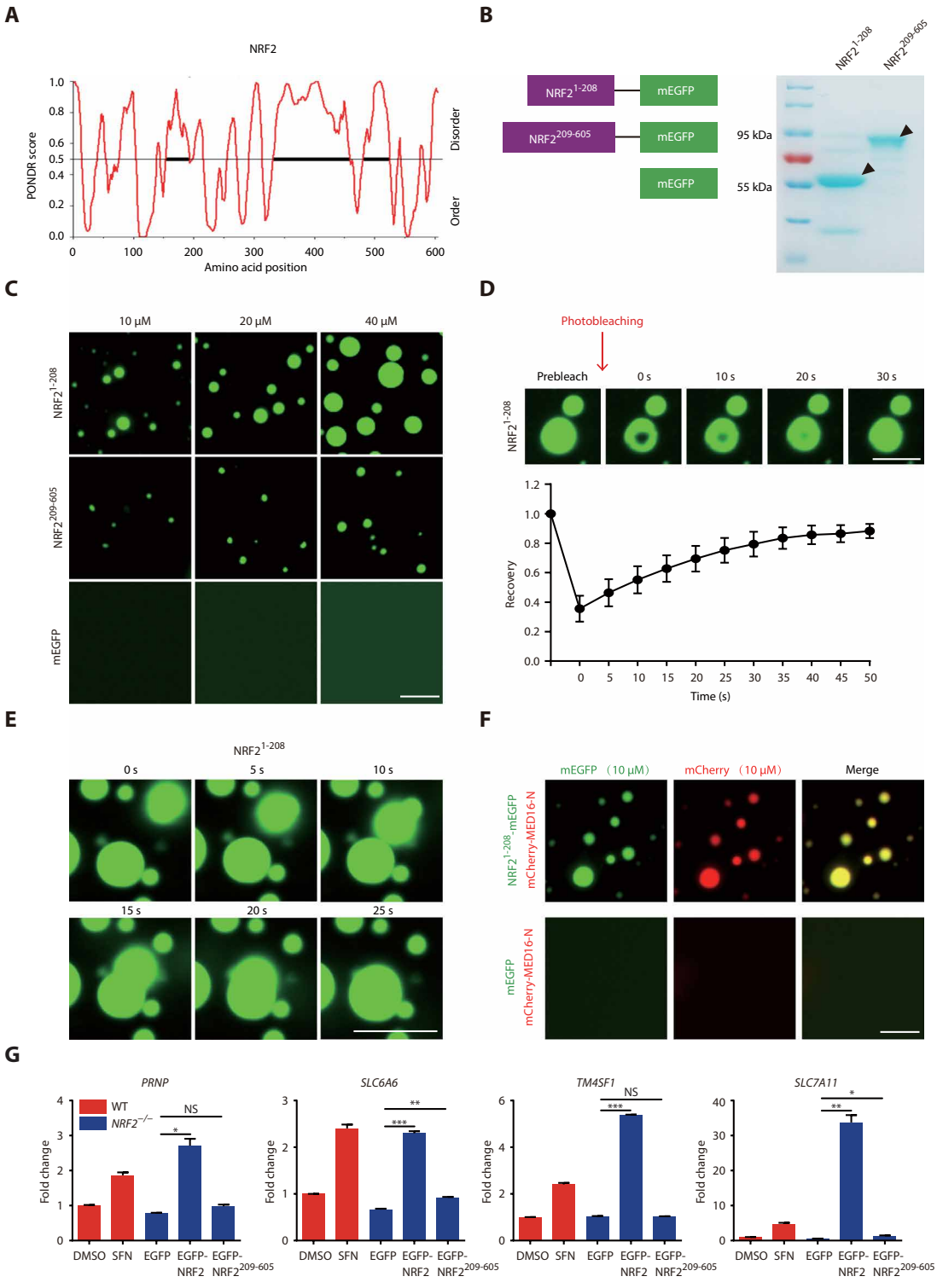

Fig. 7. NRF2 forms liquid droplets with MED16 in vitro. (**A**) Graph of intrinsic disorder of NRF2 as calculated by the VL-XT algorithm (http://pondr.com/). For PONDR prediction, a score above 0.5 indicates a high degree of disorder. Heavy bars indicate regions predicted to be intrinsically disordered. (**B**) Schematic presentation of recombinant NRF2 fragments fused to mEGFP (left). NRF2 fusion proteins resolved on an 8% SDS–polyacrylamide gel electrophoresis gel and detected by staining with Coomassie brilliant blue (right). (**C**) Representative images of droplet formation at the indicated concentrations of proteins. $NRF2^{1\text{-}208}$-mEGFP, $NRF2^{209\text{-}605}$-mEGFP, or mEGFP was added to the droplet formation buffer with 150 mM NaCl and 10% PEG-8000. Data are representative of three experiments. (**D**) FRAP measurements of $NRF2^{1\text{-}208}$-mEGFP droplets at the indicated time points (top). Normalized FRAP intensity curve of $NRF2^{1\text{-}208}$-mEGFP droplets ($n = 4$) (bottom). Data represent means ± SEM. (**E**) Fusion of $NRF2^{1\text{-}208}$-mEGFP droplets over 25 s. Data are representative of three experiments. (**F**) Representative images of droplet formation of 10 μM $NRF2^{1\text{-}208}$ and MED16-N. Data are representative of three experiments. (**G**) Quantitative RT-PCR analysis of relative mRNA expression of *PRNP*, *SLC6A6*, *TM4SF1*, and *SLC7A11* in WT 9-12 cells exposed to DMSO or SFN and WT 9-12 $NRF2^{-/-}$ cells in which the indicated constructs were expressed. Data represent means ± SEM from two experiments. Scale bars, (C to F) 5 μm. $^{*}P<0.05$, $^{**}P<0.01$, and $^{***}P < 0.001$. Two-tailed unpaired Student's *t* test was used for statistical analysis.

treatment (from 5.8 to 19.6%), suggesting that activation of NRF2 reprograms the superenhancer landscape in cystic cells. ChIP-seq analysis showed co-occupancy of NRF2 and MED1 at the superenhancers of representative NRF2 target genes upon SFN treatment and the requirement of NRF2 for MED1 recruitment to these sites as shown for the genes *EPS8L3* and *GPRIN2* in Fig. 8D. Together, these results showed that NRF2 and the Mediator complex form phase-separated condensates at superenhancers to regulate NRF2 target gene expression, including cytoprotective genes.

DISCUSSION

Mitochondrial defects, including abnormal mitochondrial membrane potential and morphology, increase the production of mitochondrial ROS in renal cystic cells of ADPKD mouse models. Consistent with previous studies (*6*, *7*, *44*), we found that expression of many antioxidant enzymes decreases in kidneys of mouse models of ADPKD. The increased ROS production and impaired antioxidant capacity together

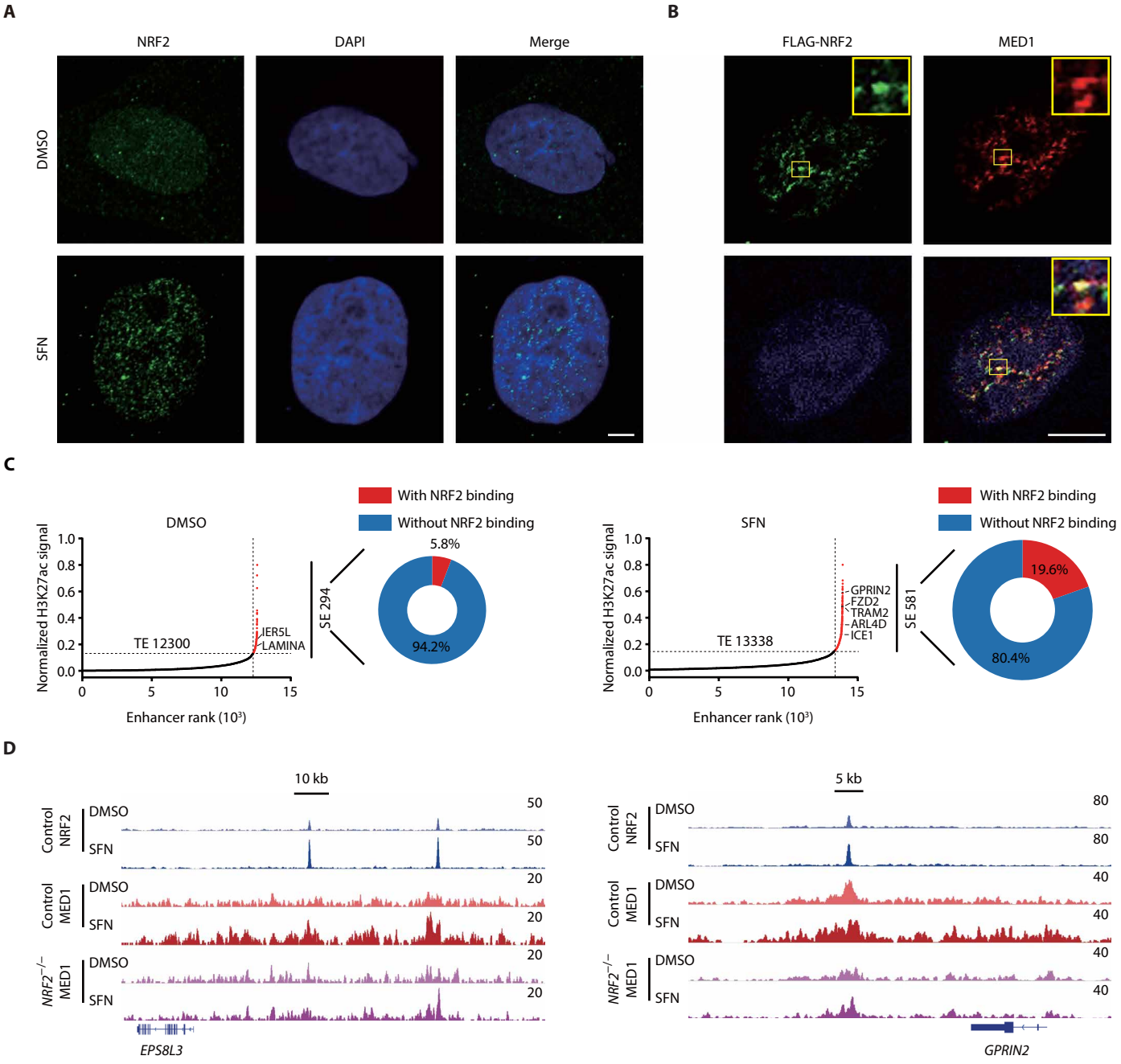

Fig. 8. NRF2 forms nuclear condensates with Mediator complex at superenhancers. (**A**) Immunofluorescence imaging of NRF2 in WT 9-12 cells with DMSO or SFN treatment. (**B**) Immunofluorescence imaging of exogenous FLAG-NRF2 and endogenous MED1. Yellow insets show a higher magnification of the indicated areas. Data in (A) and (B) are representative of three experiments. Scale bars, 5 μm. (**C**) Identification of superenhancers by the signal intensity from H3K27ac ChIP-seq. (**D**) Representative ChIP-seq profiles for NRF2 and MED1 occupancy at the indicated genes in control cells or NRF2 knockout cells with DMSO or SFN treatment.

lead to altered redox state and oxidative stress. Serum markers of oxidative stress have been reported to be higher in patients having early-stage ADPKD with preserved kidney function (*14*, *45*). Here, we provide evidence that ROS are frequently elevated in kidney tissues of patients with ADPKD and that increased ROS positively correlates with ADPKD progression. We further showed that the activity of the NRF2 antioxidant pathway is impaired in ADPKD kidneys. Pharmacological stabilization of NRF2 ameliorated oxidative stress and cyst growth in ADPKD mouse models, indicating that restoring ROS homeostasis through NRF2 activation can be effective in retarding ADPKD progression.

We determined that the repression of NRF2 antioxidant activity in cystic cells is mainly caused by increased degradation of NRF2 protein. The abundance of KEAP1 and GSK-3β are markedly increased in mouse ADPKD kidneys; this activates both KEAP1-CUL3 and β-TrCP–CUL1 degradation pathways and leads to NRF2

degradation. Inhibition of GSK-3β by TDZD-8 slows cyst expansion and disease progression in an orthologous ADPKD mouse model (*32*). However, the direct target of GSK-3β in ADPKD was hitherto unclear. We found that the anti-cystogenesis effects of TDZD-8 treatment were reduced in *Nrf2* knockout mice, indicating that NRF2 is the major target of GSK-3β in ADPKD.

The detoxification and antioxidant function of NRF2 is mainly accomplished through transcriptional activation of its cytoprotective target genes (*19*). Consistent with previous reports, we found that genome-wide NRF2 binding sites predominantly lie outside promoter-proximal regions. We showed that, in human ADPKD cells, activation of NRF2 remodels enhancer landscapes through recruitment of histone acetyltransferase P300. NRF2 enhancer occupancy correlated with the activation of its target genes, including cytoprotective genes. Our findings therefore uncover a role for the interaction between NRF2 binding and the dynamics of the chromatin environment at enhancer regions in NRF2-mediated transcriptional regulation.

We further show that the superenhancer landscape also undergoes substantial remodeling upon activation of NRF2. One prominent feature of superenhancers is the presence of phase-separated multimolecular assemblies. Phase separation is emerging as a prominent regulatory mode of transcriptional control (*37*). Transcription factors can interact with coactivator proteins, including Mediator and BRD4 (Bromodomain-containing protein 4), and form phase-separated condensates at superenhancers (*46*). Compartmentalization and concentration of the transcription apparatus by superenhancer condensates are critical for robust and simultaneous activation at multiple genes (*42*). Here, we found that the intrinsically disordered AD of NRF2 formed phase-separated droplets in vitro.

NRF2 directly interacts with the N-terminal region of the MED16 subunit of the Mediator complex, and activation of most NRF2 target genes depends on MED16 (*40*). Although MED16 does not have an IDR and the N-terminal region of MED16 does not form droplets in vitro, we showed that the NRF2-interacting domain of MED16 was readily incorporated into NRF2 liquid droplets. We found that NRF2 is required for the recruitment of the Mediator complex to superenhancers. Our pharmacological studies indicated that stabilization of NRF2 reprograms the superenhancer landscape in vivo (fig. S7D). Thus, we propose that NRF2 recruits and concentrates the transcriptional machinery to activate target genes through a phase separation mechanism at superenhancers. MED16 also regulates NRF2-dependent phosphorylation of the RNA polymerase II (Pol II) C-terminal domain (CTD) (*40*). CTD is an intrinsically disordered low-complexity region, and its phosphorylation regulates the incorporation of Pol II into different condensates formed by Mediator or splicing factors (*46*–*48*). It is currently unknown whether the phase-separating capacity of NRF2 affects Pol II CTD phosphorylation. Further research is therefore needed to investigate the role of the phase-separated environment created by NRF2 in the regulation of CTD phosphorylation and CTD-associated processes.

Some limitations of this study should be acknowledged. First, the mechanistic studies were mainly performed using an in vitro human ADPKD cell model. Although we confirmed some of the cellular findings in ADPKD mouse and human tissues, further investigation is needed to examine NRF2-mediated enhancer activation through phase separation in vivo. Second, we only tested the therapeutic effect of SFN on ADPKD progression in the late-onset mouse model, although we confirmed some of the findings and NRF2 dependency in the early-onset mouse model with TDZD-8. The effectiveness of other NRF2 stabilizers or inducers and their combination with other ADPKD treatment drugs are topics worthy of further exploration. Tolvaptan, a vasopressin 2 receptor antagonist, has recently been approved by the U.S. Food and Drug Administration for ADPKD treatment (*49*). Tolvaptan can activate NRF2 by promoting NRF2 phosphorylation by protein kinase RNA-like endoplasmic reticulum kinase (*50*). Further research is therefore needed to investigate the role of NRF2 in tolvaptan treatment of ADPKD and whether the activation of NRF2 by tolvaptan is dependent on the antagonist activity of tolvaptan on vasopressin 2 receptor. Because tolvaptan and SFN activate NRF2 through different mechanisms, it would be interesting to examine whether the combination of these drugs could generate synergistic effects for ADPKD treatment. With liver injury, a main side effect of tolvaptan during long-term use (*49*, *51*), a potential benefit of such a combination therapy may enable a reduction in the dose of tolvaptan and thus its toxicity.

In summary, we identified impaired activity of the NRF2 antioxidant pathway as a key contributor to oxidative injury and ADPKD progression. We found a phase separation-mediated mechanism by which NRF2 activates enhancers and induces target gene expression. Functional studies in the early- and late-onset ADPKD animal models provide a rationale for developing NRF2 inducers or stabilizers as potential therapeutic agents for ADPKD. A recent phase 2 clinical trial of bardoxolone methyl, another NRF2 activator, reported a clinically relevant increase in eGFR in a cohort of 31 patients with ADPKD (*52*), further supporting the NRF2-mediated antioxidant pathway as a promising therapeutic target for ADPKD. Because of its chronic and slowly progressive nature, ADPKD may need prolonged medical treatment. SFN is derived from cruciferous vegetables, and many foods contain NRF2 activators, suggesting dietary NRF2 activators as potential long-term therapeutic agents for ADPKD management (*53*, *54*).

MATERIALS AND METHODS

Study design

The objective of this study was to elucidate the mechanisms and roles of the NRF2 antioxidant pathway in redox homeostasis and cystogenesis in ADPKD. The activity of the NRF2 pathway was assessed in ADPKD mouse and human kidneys using proteomic approaches (see Supplementary Materials and Methods for details), tissue staining, and correlative analysis of NRF2 abundance with kidney function. Most data were acquired from at least three independent samples (three mice or ≥5 human tissue samples). Mechanism of NRF2-dependent changes in chromatin and gene expression were evaluated by ChIP-seq, RNA-seq, and GSEA. The ChIP-seq data were from a single biological replicate, and the RNA-seq data were from two biological replicates (see Supplementary Materials and Methods for details).

The therapeutic effects of NRF2 inducers on cyst growth were examined using early- and late-onset orthologous ADPKD mouse models. The proteomic study was performed in kidney tissues from early-onset ADPKD mouse model. The regulatory mechanisms underlying NRF2-mediated transcriptional activation were explored using genome-wide analysis and biochemical studies in an ADPKD cell culture model. Human ADPKD specimens were obtained from patients with cyst reduction surgery or nephrectomy. All patients provided informed consent, and patients' clinical biochemical

information was extracted from medical records. For animal studies with drug treatment, mice (at least $n = 5$ per group) were chosen at random for the vehicle or treatment groups. SFN (10 mg/kg) or TDZD-8 (5 mg/kg) were administered once daily for five continuous days by intraperitoneal injection after the establishment of ADPKD in the mouse models. No animals were excluded from analysis.

Continuous data were analyzed using the GraphPad Prism 7.0 software using Student's *t* test and one-way analysis of variance (ANOVA). Correlations between data of patients were analyzed using linear regression analysis and the sample Pearson's correlation coefficient. Subject-level data for experiments with $n < 20$ can be found in data file S1.

Primary cell isolation

Kidney cells were derived from WT and *Pkd1*$^{-/-}$ mice as previously described (*44*). Briefly, kidneys from the indicated mice were minced and digested using the gentle collagenase/hyaluronidase solution (STEMCELL Technologies, 07919), and 10 μg of biotinylated DBA (Vector Laboratories, B-1035) was added and incubated with gentle mixing for 10 min at 4°C for the enrichment of collecting duct cells. Then, the CELLection Biotin Binder Kit (Invitrogen, 11533D) was used to generate the single-cell solution. DBA-positive primary cells were used for RNA isolation, protein extraction, or DHE staining.

Cell culture

WT 9-12 cells were cultured as described in (*55*). Primary cells after DBA isolation were cultured in Dulbecco's modified Eagle's medium/F-12 medium supplemented with 2% fetal bovine serum, 1× insulin-transferrin-selenium (Life Technologies, 41400-045), epidermal growth factor (10 ng/ml) (Sigma-Aldrich, SRP3196), 5 μM dexamethasone (Sigma-Aldrich, D1756), 1 nM T3 (Sigma-Aldrich, T5516), and 10 mM Hepes (Sigma-Aldrich, H3375).

Immunoblotting

For Western blot analysis, kidney tissues and isolated primary cells were lysed in radioimmunoprecipitation assay lysis buffer with phosphatase inhibitor cocktail, protease inhibitor cocktail, and dithiothreitol. Antibodies used included NRF2 (Abcam, ab62352), KEAP1 (Proteintech, 10503-2-AP), GSK-3β (Cell Signaling Technology, 3D10), NQO1 (Proteintech, 11451-1-AP), α-tubulin (Proteintech, 10449-1-AP), EGFP (Santa Cruz Biotechnology, sc-8334), and Lamin B (Santa Cruz Biotechnology, sc-6216).

Immunohistochemistry

The kidney specimens were fixed in 10% formalin overnight and embedded in paraffin. Tissue microarray sections were blocked with 5% bovine serum albumin (BSA) for 1 hour and then incubated with the indicated primary antibodies [NRF2 (Abcam, ab62352), PCNA (Santa Cruz Biotechnology, sc-56), and 8-OHdG (Bioss, bs-1278R)] overnight. After incubation, kidney sections were incubated with goat anti-rabbit horseradish peroxidase secondary antibody followed by staining with the 3,3'diaminobenzidine substrate. Immunohistochemistry sections were imaged using a microscope (BX51, Olympus). For staining intensity analysis, semiquantitative *H*-score approach (*56*) was used to assess the extent of nuclear immunoreactivity of NRF2. First, staining intensity (0, 1+, 2+, or 3+) was determined for each cell in a fixed field. Second, the percentage of cells at each staining intensity level was calculated. Last, an *H*-score was assigned using the following formula: [1 × (% cells 1+) + 2 × (% cells 2+) + 3 × (% cells 3+)].

Immunofluorescence

Cells were washed twice in phosphate-buffered saline (PBS) and blocked for 1 hour in 5% BSA, and then the cells or sections were incubated with the indicated antibodies [NRF2 (Abcam, ab62352), MED1 (Bethyl, A300-793A), and FLAG (Sigma-Aldrich, F1804)] diluted in the 5% BSA solution at 4°C overnight. After primary antibody incubation, goat anti-rabbit Alexa Fluor 488 or goat anti-mouse Alexa Fluor 555 secondary antibodies (Thermo Fisher Scientific) were applied. Samples were imaged immediately with a fluorescence microscope (DMi8, Leica).

DHE staining

ROS production in primary cells or kidney tissues was evaluated using DHE staining (Invitrogen, D11347). DHE was suspended in dimethyl sulfoxide (DMSO) at a stock concentration of 10 mM and diluted for a final concentration of 20 μM in PBS before using. Cells or optimal cutting temperature–embedded kidney specimens were washed three times in PBS. After adding the DHE solution, tissue sections or cells were incubated in a light-protected humidified box at room temperature for 30 min. The slides or cells were stained with DAPI (4′,6-diamidino-2-phenylindole) and imaged immediately with a fluorescence microscope (DMi8, Leica).

RNA isolation and RT-qPCR

Total RNA was isolated form the primary cells or kidney tissues using TRIzol (Invitrogen, 15596018). Total RNA was reverse transcribed to complementary DNA (cDNA) using the cDNA Synthesis Kit (Roche, 5081955001). Real-time quantitative polymerase chain reaction (RT-qPCR) was performed using SYBR Green Master (Roche, 41472600) with the gene-specific primers (see Supplementary Materials and Methods).

Mice and drug treatment

Nrf2$^{-/-}$ mice were generated as described in (*57*). We generated *Pkd1*$^{fl/fl}$;*Nrf2*$^{-/-}$ mice by crossing *Pkd1*$^{fl/fl}$;*Cre/Esr1*$^{+}$ mice with *Nrf2*$^{-/-}$ mice. To induce *Pkd1* gene deletion, tamoxifen (Sigma-Aldrich, T5648) was freshly prepared by dissolving in corn oil (Sigma-Aldrich, C8267) and intraperitoneally injected to induce Cre recombinase activity. Tamoxifen (10 mg/kg) was administered at P10 to generate the early-onset mouse model, and tamoxifen (250 mg/kg) was injected at P25 and P28 to generate the late-onset mouse model (*58*). For drug treatment in the early-onset mouse model, the dosages of SFN (LKT Labs, S8047) (dissolved in 5% DMSO in saline) and TDZD-8 (Selleck, S2926) (dissolved in 5% DMSO in saline) were 10 and 5 mg/kg, respectively. SFN or TDZD-8 was administered once daily for five continuous days, followed by two rest days, for every 7-day period from P11 to P29. For SFN treatment in the late-onset mouse model, the same dosage and manner were used as in the early-onset model, but the administration started at P55 and continued for 2 months.

Cystic index was calculated as the cystic area to total kidney area visualized by hematoxylin and eosin–stained kidney sections. BUN was measured in the plasma samples using the QuantiChrom Urea Assay Kit (BioAssay Systems, DIUR). Creatinine was measured in the plasma samples using the QuantiChrom Creatinine Assay Kit (BioAssay Systems, DICT). All mouse care and experimental protocols were approved by the ethical committee of Tianjin Medical University (permit number SYXK 2009-00001).

Magnetic resonance imaging

Animal MRI studies were performed as previously described (*58*). Briefly, a 7-T PharmaScan 70/16 ultrashielding machine (Bruker, Switzerland) equipped with a 40-mm radio frequency was used. Isoflurane inhalation (1.5 to 2.5%) was used to anesthetize the mice, and then the animals were positioned so that the kidneys were on the center of the radiofrequency coil. The body temperature of mice was maintained at ~37°C, and the breathing was monitored by a respiratory sensor during MRI. Total kidney volume was calculated from the contiguous images.

Human subjects

ADPKD kidney specimens were obtained from patients with cyst reduction surgery or nephrectomy. All patients provided informed consent and patients' clinical biochemical information was extracted from medical records. Human studies were approved by the ethics committee of Shandong Provincial Hospital.

In vitro droplet assay

Recombinant mEGFP or mCherry fusion proteins (see Supplementary Materials and Methods) were concentrated at 10 μM. Recombinant proteins were added to the solutions at varying concentrations with 150 mM final salt and 10% PEG-8000 (polyethylene glycol, molecular weight 8000). The protein solution was loaded onto a glass slide with a coverslip. Slides were then imaged with a fluorescence microscope (DMi8, Leica).

FRAP analysis

Droplets of proteins were allowed to form. Then, samples were bleached with ZEISS LSM 800 using a 488-nM laser of a confocal microscope with a 63×/1.4 oil objective. Recovery was imaged on ZEISS LSM 800 confocal laser scanning microscope every 5 s for the indicated time periods.

Statistical analysis

All data were presented as means ± SEM. Statistical analyses were performed using GraphPad Prism 7.0 software. For normally distributed continuous variables, unpaired two-tailed Student's *t* test was used for statistical significance between two independent experimental groups, and one-way ANOVA followed by Tukey's post hoc test was used for multiple group comparison. Correlations between data on patients [ROS, total kidney volume, serum creatinine, eGFR, and NRF2 expression] were analyzed using linear regression analysis and the sample Pearson's correlation coefficient. $P \leq 0.05$ was considered statistically significant.

SUPPLEMENTARY MATERIALS

stm.sciencemag.org/cgi/content/full/12/554/eaba3613/DC1

Materials and Methods

Fig. S1. Proteomic analysis of mouse ADPKD kidneys.

Fig. S2. Immunoblot analysis of NRF2 in cytosol and nuclear fraction of WT and *Pkd1*$^{-/-}$ mouse kidneys.

Fig. S3. Loss of *Nrf2* increases oxidative stress and accelerates cystogenesis in ADPKD mouse model.

Fig. S4. SFN treatment inhibits cystogenesis in ADPKD mouse models.

Fig. S5. TDZD-8 treatment increases the expression of NRF2 targets and improves kidney function in ADPKD mice.

Fig. S6. SFN treatment increases the expression of NRF2 targets and promotes enhancer activation.

Fig. S7. NRF2 forms liquid droplets in vitro.

Table S1. Demographic and clinical information of patients.

Table S2. Single-guide RNA sequences used to knock out NRF2 by CRISPR/Cas-9 gene editing.

Data file S1. Individual subject-level data (Microsoft Excel file).

View/request a protocol for this paper from *Bio-protocol*.

REFERENCES AND NOTES

1. E. Cornec-Le Gall, A. Alam, R. D. Perrone, Autosomal dominant polycystic kidney disease. *Lancet* **393**, 919–935 (2019).
2. C. Bergmann, L. M. Guay-Woodford, P. C. Harris, S. Horie, D. J. M. Peters, V. E. Torres, Polycystic kidney disease. *Nat. Rev. Dis. Primers.* **4**, 50 (2018).
3. V. Padovano, C. Podrini, A. Boletta, M. J. Caplan, Metabolism and mitochondria in polycystic kidney disease research and therapy. *Nat. Rev. Nephrol.* **14**, 678–687 (2018).
4. L. F. Menezes, G. G. Germino, The pathobiology of polycystic kidney disease from a metabolic viewpoint. *Nat. Rev. Nephrol.* **15**, 735–749 (2019).
5. C. Podrini, L. Cassina, A. Boletta, Metabolic reprogramming and the role of mitochondria in polycystic kidney disease. *Cell. Signal.* **67**, 109495 (2019).
6. C. C. Lin, M. Kurashige, Y. Liu, T. Terabayashi, Y. Ishimoto, T. Wang, V. Choudhary, R. Hobbs, L. K. Liu, P. H. Lee, P. Outeda, F. Zhou, N. P. Restifo, T. Watnick, H. Kawano, S. Horie, W. Prinz, H. Xu, L. F. Menezes, G. G. Germino, A cleavage product of Polycystin-1 is a mitochondrial matrix protein that affects mitochondria morphology and function when heterologously expressed. *Sci. Rep.* **8**, 2743 (2018).
7. Y. Ishimoto, R. Inagi, D. Yoshihara, M. Kugita, S. Nagao, A. Shimizu, N. Takeda, M. Wake, K. Honda, J. Zhou, M. Nangaku, Mitochondrial abnormality facilitates cyst formation in autosomal dominant polycystic kidney disease. *Mol. Cell. Biol.* **37**, e00337-17 (2017).
8. H. Sies, C. Berndt, D. P. Jones, Oxidative stress. *Annu. Rev. Biochem.* **86**, 715–748 (2017).
9. P. Poprac, K. Jomova, M. Simunkova, V. Kollar, C. J. Rhodes, M. Valko, Targeting free radicals in oxidative stress-related human diseases. *Trends Pharmacol. Sci.* **38**, 592–607 (2017).
10. R. L. Maser, D. Vassmer, B. S. Magenheimer, J. P. Calvet, Oxidant stress and reduced antioxidant enzyme protection in polycystic kidney disease. *J. Am. Soc. Nephrol.* **13**, 991–999 (2002).
11. A. Tariq, M. A. Mansoor, H. P. Marti, G. Jonsson, A. Slettan, P. Weeraman, T. Apeland, Systemic redox biomarkers and their relationship to prognostic risk markers in autosomal dominant polycystic kidney disease and IgA nephropathy. *Clin. Biochem.* **56**, 33–40 (2018).
12. K. L. Nowak, W. Wang, H. Farmer-Bailey, B. Gitomer, M. Malaczewski, J. Klawitter, A. Jovanovich, M. Chonchol, Vascular dysfunction, oxidative stress, and inflammation in autosomal dominant polycystic kidney disease. *Clin. J. Am. Soc. Nephrol.* **13**, 1493–1501 (2018).
13. J. Klawitter, B. Y. Reed-Gitomer, K. McFann, A. Pennington, J. Klawitter, K. Z. Abebe, J. Klepacki, M. A. Cadnapaphornchai, G. Brosnahan, M. Chonchol, U. Christians, R. W. Schrier, Endothelial dysfunction and oxidative stress in polycystic kidney disease. *Am. J. Physiol. Ren. Physiol.* **307**, F1198–F1206 (2014).
14. T. Nakamura, E. Sato, N. Fujiwara, Y. Kawagoe, S. Yamada, Y. Ueda, H. Koide, Changes in urinary albumin excretion, inflammatory and oxidative stress markers in ADPKD patients with hypertension. *Am J Med Sci* **343**, 46–51 (2012).
15. P. Moi, K. Chan, I. Asunis, A. Cao, Y. W. Kan, Isolation of NF-E2-related factor 2 (Nrf2), a NF-E2-like basic leucine zipper transcriptional activator that binds to the tandem NF-E2/AP1 repeat of the beta-globin locus control region. *Proc. Natl. Acad. Sci. U.S.A.* **91**, 9926–9930 (1994).
16. K. Itoh, K. Igarashi, N. Hayashi, M. Nishizawa, M. Yamamoto, Cloning and characterization of a novel erythroid cell-derived CNC family transcription factor heterodimerizing with the small Maf family proteins. *Mol. Cell. Biol.* **15**, 4184–4193 (1995).
17. M. Yamamoto, T. W. Kensler, H. Motohashi, The KEAP1-NRF2 system: A thiol-based sensor-effector apparatus for maintaining redox homeostasis. *Physiol. Rev.* **98**, 1169–1203 (2018).
18. C. J. Schmidlin, M. B. Dodson, L. Madhavan, D. D. Zhang, Redox regulation by NRF2 in aging and disease. *Free Radic. Biol. Med.* **134**, 702–707 (2019).
19. C. Tonelli, I. I. C. Chio, D. A. Tuveson, Transcriptional regulation by Nrf2. *Antioxid. Redox Signal.* **29**, 1727–1745 (2018).
20. K. Itoh, N. Wakabayashi, Y. Katoh, T. Ishii, K. Igarashi, J. D. Engel, M. Yamamoto, Keap1 represses nuclear activation of antioxidant responsive elements by Nrf2 through binding to the amino-terminal Neh2 domain. *Genes Dev.* **13**, 76–86 (1999).
21. Y. Gorin, The kidney: An organ in the front line of oxidative stress-associated pathologies. *Antioxid. Redox Signal.* **25**, 639–641 (2016).
22. G. Coppolino, G. Leonardi, M. Andreucci, D. Bolignano, Oxidative stress and kidney function: A brief update. *Curr. Pharm. Des.* **24**, 4794–4799 (2018).
23. S. Ruiz, P. E. Pergola, R. A. Zager, N. D. Vaziri, Targeting the transcription factor Nrf2 to ameliorate oxidative stress and inflammation in chronic kidney disease. *Kidney Int.* **83**, 1029–1041 (2013).

24. M. Nezu, N. Suzuki, M. Yamamoto, Targeting the KEAP1-NRF2 system to prevent kidney disease progression. *Am. J. Nephrol.* **45**, 473–483 (2017).
25. P. C. Harris, V. E. Torres, Genetic mechanisms and signaling pathways in autosomal dominant polycystic kidney disease. *J. Clin. Invest.* **124**, 2315–2324 (2014).
26. D. E. Handy, J. Loscalzo, Redox regulation of mitochondrial function. *Antioxid. Redox Signal.* **16**, 1323–1367 (2012).
27. P. A. Andreux, R. H. Houtkooper, J. Auwerx, Pharmacological approaches to restore mitochondrial function. *Nat. Rev. Drug Discov.* **12**, 465–483 (2013).
28. T. W. Kensler, P. A. Egner, A. S. Agyeman, K. Visvanathan, J. D. Groopman, J. G. Chen, T. Y. Chen, J. W. Fahey, P. Talalay, Keap1-nrf2 signaling: A target for cancer prevention by sulforaphane. *Top. Curr. Chem.* **329**, 163–177 (2013).
29. C. A. Houghton, Sulforaphane: Its "coming of age" as a clinically relevant nutraceutical in the prevention and treatment of chronic disease. *Oxidative Med. Cell. Longev.* **2019**, 2716870 (2019).
30. M. Chiaravalli, I. Rowe, V. Mannella, G. Quilici, T. Canu, V. Bianchi, A. Gurgone, S. Antunes, P. D'Adamo, A. Esposito, G. Musco, A. Boletta, 2-Deoxy-d-glucose ameliorates PKD progression. *J. Am. Soc. Nephrol.* **27**, 1958–1969 (2016).
31. L. F. M. van de Laarschot, J. P. H. Drenth, Genetics and mechanisms of hepatic cystogenesis. *Biochim. Biophys. Acta Mol. basis Dis.* **1864**, 1491–1497 (2018).
32. S. Tao, V. R. Kakade, J. R. Woodgett, P. Pandey, E. D. Suderman, M. Rajagopal, R. Rao, Glycogen synthase kinase-3beta promotes cyst expansion in polycystic kidney disease. *Kidney Int.* **87**, 1164–1175 (2015).
33. Y. Hirotsu, F. Katsuoka, R. Funayama, T. Nagashima, Y. Nishida, K. Nakayama, J. D. Engel, M. Yamamoto, Nrf2-MafG heterodimers contribute globally to antioxidant and metabolic networks. *Nucleic Acids Res.* **40**, 10228–10239 (2012).
34. B. N. Chorley, M. R. Campbell, X. Wang, M. Karaca, D. Sambandan, F. Bangura, P. Xue, J. Pi, S. R. Kleeberger, D. A. Bell, Identification of novel NRF2-regulated genes by ChIP-Seq: Influence on retinoid X receptor alpha. *Nucleic Acids Res.* **40**, 7416–7429 (2012).
35. ENCODE Project Consortium, An integrated encyclopedia of DNA elements in the human genome. *Nature* **489**, 57–74 (2012).
36. Z. Sun, Y. E. Chin, D. D. Zhang, Acetylation of Nrf2 by p300/CBP augments promoter-specific DNA binding of Nrf2 during the antioxidant response. *Mol. Cell. Biol.* **29**, 2658–2672 (2009).
37. D. Hnisz, K. Shrinivas, R. A. Young, A. K. Chakraborty, P. A. Sharp, A phase separation model for transcriptional control. *Cell* **169**, 13–23 (2017).
38. A. Boija, I. A. Klein, B. R. Sabari, A. Dall'Agnese, E. L. Coffey, A. V. Zamudio, C. H. Li, K. Shrinivas, J. C. Manteiga, N. M. Hannett, B. J. Abraham, L. K. Afeyan, Y. E. Guo, J. K. Rimel, C. B. Fant, J. Schuijers, T. I. Lee, D. J. Taatjes, R. A. Young, Transcription factors activate genes through the phase-separation capacity of their activation domains. *Cell* **175**, 1842–1855.e16 (2018).
39. Y. Shin, C. P. Brangwynne, Liquid phase condensation in cell physiology and disease. *Science* **357**, eaaf4382 (2017).
40. H. Sekine, K. Okazaki, N. Ota, H. Shima, Y. Katoh, N. Suzuki, K. Igarashi, M. Ito, H. Motohashi, M. Yamamoto, The mediator subunit MED16 transduces NRF2-activating signals into antioxidant gene expression. *Mol. Cell. Biol.* **36**, 407–420 (2016).
41. B. R. Sabari, A. Dall'Agnese, A. Boija, I. A. Klein, E. L. Coffey, K. Shrinivas, B. J. Abraham, N. M. Hannett, A. V. Zamudio, J. C. Manteiga, C. H. Li, Y. E. Guo, D. S. Day, J. Schuijers, E. Vasile, S. Malik, D. Hnisz, T. I. Lee, I. I. Cisse, R. G. Roeder, P. A. Sharp, A. K. Chakraborty, R. A. Young, Coactivator condensation at super-enhancers links phase separation and gene control. *Science* **361**, eaar3958 (2018).
42. W. A. Whyte, D. A. Orlando, D. Hnisz, B. J. Abraham, C. Y. Lin, M. H. Kagey, P. B. Rahl, T. I. Lee, R. A. Young, Master transcription factors and mediator establish super-enhancers at key cell identity genes. *Cell* **153**, 307–319 (2013).
43. H. Y. Shin, Targeting super-enhancers for disease treatment and diagnosis. *Mol. Cells* **41**, 506–514 (2018).
44. L. F. Menezes, C. C. Lin, F. Zhou, G. G. Germino, Fatty acid oxidation is impaired in an orthologous mouse model of autosomal dominant polycystic kidney disease. *EBioMedicine* **5**, 183–192 (2016).
45. V. Menon, D. Rudym, P. Chandra, D. Miskulin, R. Perrone, M. Sarnak, Inflammation, oxidative stress, and insulin resistance in polycystic kidney disease. *Clin. J. Am. Soc. Nephrol.* **6**, 7–13 (2011).
46. W.-K. Cho, J. H. Spille, M. Hecht, C. Lee, C. Li, V. Grube, I. I. Cisse, Mediator and RNA polymerase II clusters associate in transcription-dependent condensates. *Science* **361**, 412–415 (2018).
47. H. Lu, D. Yu, A. S. Hansen, S. Ganguly, R. Liu, A. Heckert, X. Darzacq, Q. Zhou, Phase-separation mechanism for C-terminal hyperphosphorylation of RNA polymerase II. *Nature* **558**, 318–323 (2018).
48. Y. E. Guo, J. C. Manteiga, J. E. Henninger, B. R. Sabari, A. Dall'Agnese, N. M. Hannett, J.-H. Spille, L. K. Afeyan, A. V. Zamudio, K. Shrinivas, B. J. Abraham, A. Boija, T.-M. Decker, J. K. Rimel, C. B. Fant, T. I. Lee, I. I. Cisse, P. A. Sharp, D. J. Taatjes, R. A. Young, Pol II phosphorylation regulates a switch between transcriptional and splicing condensates. *Nature* **572**, 543–548 (2019).
49. F. T. Chebib, R. D. Perrone, A. B. Chapman, N. K. Dahl, P. C. Harris, M. Mrug, R. A. Mustafa, A. Rastogi, T. Watnick, A. S. L. Yu, V. E. Torres, A practical guide for treatment of rapidly progressive ADPKD with tolvaptan. *J. Am. Soc. Nephrol.* **29**, 2458–2470 (2018).
50. T. Fujiki, F. Ando, K. Murakami, K. Isobe, T. Mori, K. Susa, N. Nomura, E. Sohara, T. Rai, S. Uchida, Tolvaptan activates the Nrf2/HO-1 antioxidant pathway through PERK phosphorylation. *Sci. Rep.* **9**, 9245 (2019).
51. M. Mosedale, Y. Kim, W. J. Brock, S. E. Roth, T. Wiltshire, J. S. Eaddy, G. R. Keele, R. W. Corty, Y. Xie, W. Valdar, P. B. Watkins, Editor's highlight: Candidate risk factors and mechanisms for tolvaptan-induced liver injury are identified using a collaborative cross approach. *Toxicol. Sci.* **156**, 438–454 (2017).
52. P. Pergola, A. Acharya, G. Appel, A. Awad, J. Betts, G. Block, M. Chin, A. Goldsberry, L. Inker, C. Meyer, A. Rastogi, D. Rizk, K. Schroeder, C. Wanner, A. Silva, Safety and efficacy of bardoxolone methyl in patients with rare chronic kidney diseases. *Nephrol. Dial. Transplant.* **34**, (2019).
53. H. Kumar, I. S. Kim, S. V. More, B. W. Kim, D. K. Choi, Natural product-derived pharmacological modulators of Nrf2/ARE pathway for chronic diseases. *Nat. Prod. Rep.* **31**, 109–139 (2014).
54. A. Cuadrado, A. I. Rojo, G. Wells, J. D. Hayes, S. P. Cousin, W. L. Rumsey, O. C. Attucks, S. Franklin, A. L. Levonen, T. W. Kensler, A. T. Dinkova-Kostova, Therapeutic targeting of the NRF2 and KEAP1 partnership in chronic diseases. *Nat. Rev. Drug Discov.* **18**, 295–317 (2019).
55. C. Liu, H. Li, X. Gao, M. Yang, L. Yuan, L. Fu, X. Wang, C. Mei, Concomitant use of rapamycin and rosiglitazone delays the progression of polycystic kidney disease in Han:SPRD rats: A study of the mechanism of action. *Am. J. Physiol. Ren. Physiol.* **314**, F844–F854 (2018).
56. A. A. Thike, M. J. Chng, P. H. Tan, S. Fook-Chong, Immunohistochemical expression of hormone receptors in invasive breast carcinoma: Correlation of results of H-score with pathological parameters. *Pathology* **33**, 21–25 (2001).
57. K. Itoh, T. Chiba, S. Takahashi, T. Ishii, K. Igarashi, Y. Katoh, T. Oyake, N. Hayashi, K. Satoh, I. Hatayama, M. Yamamoto, Y.-i. Nabeshima, An Nrf2/small Maf heterodimer mediates the induction of phase II detoxifying enzyme genes through antioxidant response elements. *Biochem. Biophys. Res. Commun.* **236**, 313–322 (1997).
58. Y. Sun, Z. Liu, X. Cao, Y. Lu, Z. Mi, C. He, J. Liu, Z. Zheng, M. J. Li, T. Li, D. Xu, M. Wu, Y. Cao, Y. Li, B. Yang, C. Mei, L. Zhang, Y. Chen, Activation of P-TEFb by cAMP-PKA signaling in autosomal dominant polycystic kidney disease. *Sci. Adv.* **5**, eaaw3593 (2019).

Acknowledgments: Editorial services were provided by N. Gough (BioSerendipity LLC, Elkridge, MD). **Funding:** This work was supported by grants (81770658 and 31571337 to Y.C., 31571336 to L.Z., and 31601111 to X.Z.) from the National Natural Science Foundation of China, a grant (2017YFA0504102 to Y.C.) from the National Key Research and Development Program of China, a grant (to Y.C.) from the Excellent Talent Project of Tianjin Medical University, and a grant (2019GSF107050 to H.X.) from the Shandong Key Research and Development Program. **Author contributions:** Yi Lu performed mouse and biochemistry studies. Y.S. performed human specimen analysis and mouse studies. Z.L. performed bioinformatics analysis. Yumei Lu provided expertise on phase separation analysis. X.Z. performed bioinformatics analysis. B.L. assisted with the biochemical studies. Z.M. performed the immunostaining. L.D. performed ChIP-seq analysis. N.L. performed biochemistry studies. W.Z. performed mouse studies. L.T. provided expertise on mouse studies. J.P. provided *Nrf2* knockout mice. H.X. provided human specimens and edited the manuscript. L.Z. and Y.C. conceived, designed, and supervised the project, analyzed data, and wrote the manuscript. **Competing interests:** The authors declare that they have no competing interests. **Data and materials availability:** All data associated with this study are present in the paper or the Supplementary Materials. The proteomic data can be accessed in the PRIDE archive under the accession number PXD016312. RNA-seq and ChIP-seq data are deposited to Gene Expression Omnibus under accession number GSE141741.

Submitted 27 November 2019
Accepted 8 April 2020
Published 29 July 2020
10.1126/scitranslmed.aba3613

Citation: Y. Lu, Y. Sun, Z. Liu, Y. Lu, X. Zhu, B. Lan, Z. Mi, L. Dang, N. Li, W. Zhan, L. Tan, J. Pi, H. Xiong, L. Zhang, Y. Chen, Activation of NRF2 ameliorates oxidative stress and cystogenesis in autosomal dominant polycystic kidney disease. *Sci. Transl. Med.* **12**, eaba3613 (2020).

Science Translational Medicine

Activation of NRF2 ameliorates oxidative stress and cystogenesis in autosomal dominant polycystic kidney disease

Yi Lu, Yongzhan Sun, Zhiheng Liu, Yumei Lu, Xu Zhu, Bingxue Lan, Zeyun Mi, Lin Dang, Na Li, Wenlei Zhan, Lu Tan, Jingbo Pi, Hui Xiong, Lirong Zhang and Yupeng Chen

Sci Transl Med **12**, eaba3613.
DOI: 10.1126/scitranslmed.aba3613

Antioxidants dominate ADPKD

Autosomal dominant polycystic kidney disease (ADPKD) is a relatively common genetic disorder whose pathogenesis is only partially understood. By studying both human patients and mouse models, Lu *et al*. identified inactivating mutations of the antioxidant protein NRF2 as playing a key role in the pathogenesis of this disorder. In addition to clarifying the mechanism of disease development, the authors demonstrated that pharmacologic induction of the NRF2 pathway slows the progression of disease in mouse models, suggesting a potential intervention for human patients.

Science Translational Medicine (ISSN 1946-6242) is published by the American Association for the Advancement of Science, 1200 New York Avenue NW, Washington, DC 20005. The title *Science Translational Medicine* is a registered trademark of AAAS.